

UC Santa Cruz

UC Santa Cruz Electronic Theses and Dissertations

Title

Identifying and tracking evolving water masses in optically complex aquatic environments

Permalink

<https://escholarship.org/uc/item/19c9r3w1>

Author

Palacios, Sherry Lynn

Publication Date

2012

Peer reviewed|Thesis/dissertation

UNIVERSITY OF CALIFORNIA
SANTA CRUZ
**IDENTIFYING AND TRACKING EVOLVING WATER MASSES
IN OPTICALLY COMPLEX AQUATIC ENVIRONMENTS**

A dissertation submitted in partial satisfaction
of the requirements for the degree of
DOCTOR OF PHILOSOPHY

in
OCEAN SCIENCES
by

Sherry L. Palacios

March 2012

The Dissertation of Sherry L. Palacios
is approved:

Professor Raphael M. Kudela, Chair

Professor Christopher A. Edwards

Professor G. Jason Smith

Tyrus Miller
Vice Provost and Dean of Graduate Studies

Copyright © by

Sherry L. Palacios

2012

TABLE OF CONTENTS

Table of Contents.....	iii
List of Figures.....	v
List of Tables.....	vii
Abstract.....	ix
Dedication.....	xi
Acknowledgements.....	xii
Introduction.....	1
Chapter 1 : Development of synthetic salinity from remote sensing for the Columbia River Plume.....	16
Abstract.....	16
Introduction.....	17
Methods.....	21
Results.....	32
Discussion.....	47
Literature Cited.....	53
Chapter 2 : Optical characterization of water masses within the Columbia River Plume	58
Abstract.....	58
Introduction.....	59
Methods.....	65

Results.....	75
Discussion.....	100
Literature Cited.....	109
Chapter 3 : Discrimination of phytoplankton taxa in an optically complex aquatic environment.....	113
Abstract.....	113
Introduction.....	114
Methods.....	127
Results.....	144
Discussion.....	167
Literature Cited.....	178
Conclusions.....	186

LIST OF FIGURES

Introduction

Figure 1.....10

Figure 2.....12

Chapter 1: Development of synthetic salinity from remote sensing for the Columbia River Plume

Figure 1.122

Figure 1.223

Figure 1.326

Figure 1.434

Figure 1.538

Figure 1.639

Figure 1.742

Figure 1.843

Figure 1.945

Chapter 2: Optical characterization of water masses within the Columbia River Plume

Figure 2.165

Figure 2.267

Figure 2.377

Figure 2.485

Figure 2.587

Figure 2.6	89
Figure 2.7	91
Figure 2.8	93
Chapter 3: Discrimination of phytoplankton taxa in an optically complex aquatic environment	
Figure 3.1	124
Figure 3.2	128
Figure 3.3	146
Figure 3.4	147
Figure 3.5	149
Figure 3.6	151
Figure 3.7	152
Figure 3.8	163
Figure 3.9	165
Figure 3.10.....	166

LIST OF TABLES

Chapter 1: Development of synthetic salinity from remote sensing for the Columbia River Plume	
Table 1.1.....	29
Table 1.2.....	31
Table 1.3.....	35
Table 1.4.....	35
Table 1.5.....	46
Chapter 2: Optical characterization of water masses within the Columbia River Plume	
Table 2.1.....	68
Table 2.2.....	79
Table 2.3.....	80
Table 2.4.....	82
Table 2.5.....	83
Table 2.6.....	95
Table 2.7.....	99
Chapter 3: Discrimination of phytoplankton taxa in an optically complex aquatic environment	
Table 3.1.....	129
Table 3.2.....	137

Table 3.3.....	154
Table 3.4.....	156
Table 3.5.....	158
Table 3.6.....	158
Table 3.7.....	159
Table 3.8.....	162
Table 3.9.....	164

CHAPTER 3

Discrimination of phytoplankton taxa in an optically complex aquatic environment

Abstract

A new hyperspectral bio-optical algorithm has been developed to discriminate phytoplankton taxa in optically complex, case 2 waters. The semi-analytical, phytoplankton detection with optics (PHYDOTax) algorithm is based on first principles of bio-optics with possible applications to biogeochemical modeling, testing of plankton functional type (PFT) models, and detection and monitoring of harmful algal blooms. A signature library of remote sensing reflectance (R_{rs}) spectra for seven major phytoplankton groups (diatoms, dinoflagellates, haptophytes, chlorophytes, cryptophytes, cyanophytes, and unspecified phycocyanin-containing picoeukaryotes – UPCE) was developed using measured and modeled inherent optical properties as inputs to the radiative transfer equations. Normalized R_{rs} spectra were sub-setted to 10 nm resolution from 455 nm to 675 nm to create the signature library. This library and the inverse-matrix-based decomposition algorithm, PHYDOTax, were used to discriminate taxon-specific biomass in both synthetic phytoplankton mixtures and field samples from Monterey Bay, CA in 2006, 2008, 2009, and 2010. Validation with the synthetic mixtures showed strong correlation between algorithm predictions and known mixture proportions for all taxa but one, *Emiliana huxleyi*. Field validation demonstrated a strong correlation between measured and modeled taxon-specific biomass for diatoms, dinoflagellates, haptophytes, chlorophytes, and

UPCE (but not cryptophytes). Cyanophytes could not be field validated. PHYDOTax was applied to hyperspectral imagery for the Monterey Bay in 2006 and the algorithm predicted a dominant dinoflagellate bloom ($> 60\%$ of chlorophyll-*a* biomass) with relatively high diatom biomass within the bloom ($\sim 20\%$ of chlorophyll-*a* biomass) and at the periphery of the bloom; a pattern confirmed with *in situ* cell counts. PHYDOTax is unique in that it can discriminate between dinoflagellates and diatoms, a distinction historically considered challenging using chlorophyll-*a*, pigments, or light absorption spectra alone. With increased availability of hyperspectral remote sensing imagery on existing satellites, and the launch of new satellites, PHYDOTax holds promise for validating plankton functional type models, modeling biogeochemical cycles, and monitoring harmful algae in optically complex coastal waters.

Key Terms: PHYDOTax, hyperspectral, phytoplankton discriminator, harmful algal bloom (HAB), plankton functional type (PFT)

1. Introduction

1.1 Ocean Color Remote Sensing

The age of ocean color remote sensing began in 1978 with the deployment of the Nimbus-7 satellite and Coastal Zone Color Scanner (CZCS) ocean color imager [Gordon *et al.*, 1983]. The initial goal of ocean color remote sensing was to estimate global chlorophyll- *a* biomass [O'Reilly *et al.*, 1998]. Early work focused on open-

ocean, case 1 waters where phytoplankton dominates ocean color compared with the contribution by inorganic particles [*Morel and Prieur*, 1977]. More sophisticated algorithms were developed to estimate chlorophyll-*a* in optically complex, case 2 waters [*Carder et al.*, 1989], where chlorophyll-*a* contributes less than inorganic particles to ocean color. Chromophoric dissolved organic matter (CDOM) is present in both case 1 and case 2 water, but generally does not co-vary with chlorophyll-*a* in case 2 waters. With credible chlorophyll-*a* biomass estimates for both case 1 and case 2 waters, we have a more thorough understanding of global ecosystem dynamics, climate processes, and ocean circulation. Ocean color algorithms have expanded in scope and number, beyond just bulk chlorophyll-*a* estimates, to include the determination of inherent optical properties (IOPs) [*Lee et al.*, 2002], primary productivity [*Behrenfeld and Falkowski*, 1997], water mass detection [*Martin Traykovski and Sosik*, 2003], cell bio-volume [*Kostadinov et al.*, 2009], and red-tide indices [*Ahn and Shanmugam*, 2006]. As the study of ocean color moves to the next generation, even more complex questions are being asked. We know the phytoplankton community is there, now we wish to know who the occupants are. Ocean color algal discriminators can be used to resolve this question.

1.2 Algal Discriminators

Algal discrimination has a rich and varied history that pre-dates ocean color satellite observations and has expanded substantially in recent years [*Nair et al.*, 2008]. Many algorithms exist and this is a product of their development – usually

empirically, for a specific geographic region in order to answer specific questions.

Algal discriminator algorithms can be grouped into two major types: Those that distinguish size-class-- pico-, nano-, and micro-plankton, and those that distinguish taxon abundance [Nair *et al.*, 2008]. The reason for the dichotomy stems from the application of the algorithms. Phytoplankton size-class corresponds to ecological functional type, and these algorithms are applied primarily to biogeochemical modeling questions [Nair *et al.*, 2008]. Algorithms that discriminate taxon abundance are used for ecological modeling, but also in harmful algal bloom detection and monitoring. Some examples of both types of algal discriminator algorithms include: patterns in chlorophyll-*a* anomaly over time [Hu *et al.*, 2005], pigment ratios in whole water samples (i.e. CHEMTAX) [Mackey *et al.*, 1996], light absorption spectral shape [Ciotti *et al.*, 2002; Sathyendranath *et al.*, 2004a; Sathyendranath *et al.*, 2004b], the relationship of backscattering to chlorophyll-*a* to detect the toxic dinoflagellate *Karenia brevis* [Cannizzaro *et al.*, 2009], the relationship of remote sensing reflectance (R_{rs}) to chlorophyll-*a* to detect red-tides in optically complex waters [Ahn and Shanmugam, 2006], the spectral shape of R_{rs} [Craig *et al.*, 2006], and the relationship between the spectral shape of water leaving radiance (L_w) to diagnostic pigment bio-markers [Alvain *et al.*, 2005]. In addition to size-class or taxon algorithms, other algorithms, not detailed in this study, classify water masses with characteristics of particular algal taxa as well as other optical properties (e.g. high turbidity or CDOM) [Hommersom *et al.*, 2011; Martin Traykovski and Sosik, 2003; Moore *et al.*, 2001].

The types of questions that can be asked with algal discriminators are varied. Can observations of phytoplankton taxa from remote sensing data validate plankton functional (PFT) type models? Can carbon flow through different ecological pathways be quantified starting with observations of phytoplankton taxa in remote sensing imagery? Can carbon export estimates be better constrained, and how might this influence climate models? Can remote observations of phytoplankton taxa be used to identify and track harmful algal blooms (HABs)?

To illustrate, size-class can be modeled from ocean color remote sensing data. These size-class algorithms generally are based upon the spectral shape of a particular inherent optical property (IOP), such as light absorption or backscattering, or on the concentration of chlorophyll-*a* and other bio-marker pigments of particular phytoplankton taxa [Claustre, 1994; Devred *et al.*, 2011; Uitz *et al.*, 2006]. The spectral shape of light absorption [Ciotti *et al.*, 2002] or the composition of pigment bio-markers [Ciotti *et al.*, 1999; Sathyendranath *et al.*, 2001; Uitz *et al.*, 2006] are used to infer phytoplankton size-class based on trends found in empirical data. Though there are limitations (e.g. package effect or overlap of pigments among taxa), these methods do differentiate pico-, nano-, and micro- plankton in natural samples collected either *in situ* or from ocean color imagery. These algorithms are suitable for biogeochemical modeling, or for validating plankton functional type models that require no more than three phytoplankton size-classes. However, for more complex treatment of the phytoplankton, observations of more than these three size-classes are needed.

In comparison, taxon-specific biomass can be discriminated from ocean color remote sensing data. These estimates are useful for biogeochemical modeling, validation of plankton functional type models, and to monitor for harmful algae. Similar to size-class algorithms, taxon-specific composition of natural waters can be inferred from ocean color in several ways: by the spectral shape of IOPs such as light absorption [Sathyendranath *et al.*, 2004b; Subramaniam *et al.*, 2002] and backscattering [Cannizzaro *et al.*, 2008] and by the relationship of spectral shape of the surface L_w or R_{rs} to accessory pigment concentration [Alvain *et al.*, 2005]. This last classification algorithm, PHYSAT, is based on empirical methods and can discriminate among five major phytoplankton groups: haptophytes, *Prochlorococcus*, *Synechococcus*-like, diatoms, and *Phaeocystis*-like [Alvain *et al.*, 2005; Alvain *et al.*, 2008]. Algorithms such as PHYSAT attempt to refute the accusation that ecological modelers are “running before they can walk” [T R Anderson, 2005] by identifying plankton functional types through satellite observations that can be used to validate those models. PHYSAT is limited to case 1 waters, was built using empirical relationships, and at present only distinguishes between two major taxa in the larger size-class (haptophytes and diatoms). These limitations prevent it from being applied convincingly to case 2 waters of the coastal ocean where higher nutrient concentrations support diverse populations of phytoplankton in the microplankton size-class. These phytoplankton include diatoms, dinoflagellates, some haptophytes and cryptophytes. These larger, coastal taxa are inherently difficult to discriminate from each other because of similarities in light absorption spectra or in the overlap of

pigments among groups due to shared evolutionary ancestors [Dierssen *et al.*, 2006; Falkowski *et al.*, 2004; Keeling, 2004; Lewitus *et al.*, 2005].

Taxon-specific algal discriminators are promising tools to synoptically monitor for harmful algae with remote sensing imagery. Harmful algal blooms (HABs) are algal blooms that have deleterious effects on human or commercial activities [D M Anderson *et al.*, 2000] and are monitored to mitigate negative impacts. Because of costs and time delays, new methods have evolved to monitor HABs at larger spatial scales or higher temporal resolution in near real-time as a complement to existing agency and volunteer monitoring networks. Some of these new methods include instrumented mooring arrays that collect data relevant to HAB detection [C Scholin *et al.*, 2009], ocean color remote sensing imagery [Stumpf, 2001], and data assimilation techniques to aid HAB prediction [Stumpf *et al.*, 2003].

In situ moorings and satellite imagery provide high-resolution temporal and spatial data useful for monitoring HABs [C Scholin *et al.*, 2009; Stumpf *et al.*, 2003]. Several satellite algorithms have been developed to detect and monitor for the neuro-toxic dinoflagellate *Karenia brevis*, which forms dense blooms on the West Florida Shelf (WFS), a case 1 body of water. These algorithms include a chlorophyll-*a* anomaly [Hu *et al.*, 2005], spectral light absorption similarity index [Millie *et al.*, 1997], backscattering relationship to chlorophyll-*a* [Cannizzaro *et al.*, 2008; Cannizzaro *et al.*, 2009], and a red-tide index from an ocean color band-ratio method [Shanmugam, 2011]. The *K. brevis* work on the WFS has borne a group of bio-optical models that provide a robust test of algal discrimination in a relatively simple

optical environment. In more optically complex, case 2 waters, with multiple phytoplankton taxa, some of these methods would be less successful. One study [*Ahn and Shanmugam, 2006*] found good agreement with the red-tide index developed for the eutrophic waters in the region of the Yellow Sea of northeast Asia. This algorithm successfully discriminates a red-tide upon a background of detritus, CDOM, and chlorophyll-*a*. A second iteration of this algorithm was tested in both eutrophic and oligotrophic waters and it also successfully identified the red-tide despite some limitations due to errors in satellite-derived chl-*a* estimates [*Shanmugam, 2011*].

These red-tide indices are effective at defining one dominant bloom taxon, but they are insensitive to distinguishing more than one taxon that may compose the HAB at one time. A real need exists for an algorithm that simultaneous solves for multiple phytoplankton taxa in coastal waters. A semi-analytical phytoplankton discriminator algorithm may be a better approach to answering a wider range of questions in a flexible and credible way because it combines the generality afforded by using first principles of bio-optics, with the specificity of taxon-specific measurements of inherent optical properties.

1.3 Optics

In order to build an algorithm to detect phytoplankton taxa using first principles of bio-optics, it is important to first understand some basic concepts. Remote sensing reflectance, $R_{rs}(\lambda)$, is the quantity of ocean color detected at the sea surface by the imaging sensor aboard a ship, an airborne, or satellite platform. It is

defined as the ratio of water leaving radiance, $L_w(\lambda, 0^+)$ to downwelling irradiance, $E_d(\lambda, 0^+)$, just above the air-sea interface (Equation 1):

$$R_{rs}(\lambda) = \frac{L_w(\lambda, 0^+)}{E_d(\lambda, 0^+)} \quad (1)$$

Remote sensing reflectance is also defined in terms of the inherent and apparent optical properties of an optically deep and vertically homogeneous water column using radiative transfer theory (Equation 2):

$$R_{rs}(\lambda) = \frac{t^2}{n^2} \frac{f}{Q(\lambda)} \frac{b_b(\lambda)}{a(\lambda) + b_b(\lambda)} \quad (2)$$

where t is the transmittance across the air-seawater interface, n is the index of refraction of seawater, f is a function of the solar zenith angle, $Q(\lambda)$ is the upwelling irradiance-to-radiance ratio, $b_b(\lambda)$ is the spectral backscattering coefficient, and $a(\lambda)$ is the total spectral absorption coefficient (Lee et al. 1994). Equation 2 can be simplified to (Equation 3):

$$R_{rs}(\lambda) = C \frac{b_b(\lambda)}{a(\lambda) + b_b(\lambda)} \quad (3)$$

where C is a constant to account for transmittance across the air-sea interface, the index of refraction, the solar zenith angle, and the upwelling irradiance-to-radiance ratio. The total spectral absorption coefficient can be further decomposed to (Equation 4):

$$a(\lambda) = a_w(\lambda) + a_{NAP}(\lambda) + a_{ph}(\lambda) + a_{CDOM}(\lambda) \quad (4)$$

where the subscripts w, NAP, ph, and CDOM refer to: water, non-algal particles (detritus), phytoplankton, and chromophoric dissolved organic matter. The backscattering coefficient can be further defined (Equation 5):

$$b_b(\lambda) = b_{bw}(\lambda) + b_{bp}(\lambda) \quad (5)$$

where the subscripts w and p refer to water and particles. The radiative transfer equations (RTE) can be solved using measured inputs for the absorbing and scattering properties of the water body (e.g. $a_{NAP}(\lambda)$, a_{ph} , $a_{CDOM}(\lambda)$, $b_{bp}(\lambda)$, and the scattering phase function; with $b_{bw}(\lambda)$ and $a_w(\lambda)$ supplied from published values [*Pope and Fry, 1997*]), the nature of the wind-blown sea surface, the reflectance properties of the bottom of the water column, and the incident sun- and sky-radiance [*C.D. Mobley, 1994; C. D. Mobley and Sundman, 2008*].

The radiative transfer equations are used to solve for the spectral radiance distribution within some defined column of water. The magnitude of $a(\lambda)$ is generally much larger than $b_b(\lambda)$ in natural, open-ocean and coastal waters. Early algal discriminators rely only on variability in $a(\lambda)$ [Craig *et al.*, 2006; Millie *et al.*, 1997; Sathyendranath *et al.*, 2004a]. However, despite its relatively low magnitude, $b_b(\lambda)$ is an important variable in conferring brightness and quality to the remote sensing reflectance, and should not be ignored [Dierssen *et al.*, 2006]. Phytoplankton groups containing similar pigments and therefore having similar absorption properties could differ greatly in backscattering due to differences in size (bio-volume) or composition of the cell wall [Kirk, 1994]. Remote sensing reflectance, or alternatively normalized water leaving radiance, incorporates both the $a(\lambda)$ and $b_b(\lambda)$ components of light and therefore may be a better variable to use instead of light absorption when discriminating among similar algal taxa. This is especially true when differentiating among members of the “brown” algal taxa defined by Beutler *et al.* [Beutler *et al.*, 2002]. These taxa coexist in mixed assemblages in the case 2 waters of Monterey Bay, CA where the present study is located.

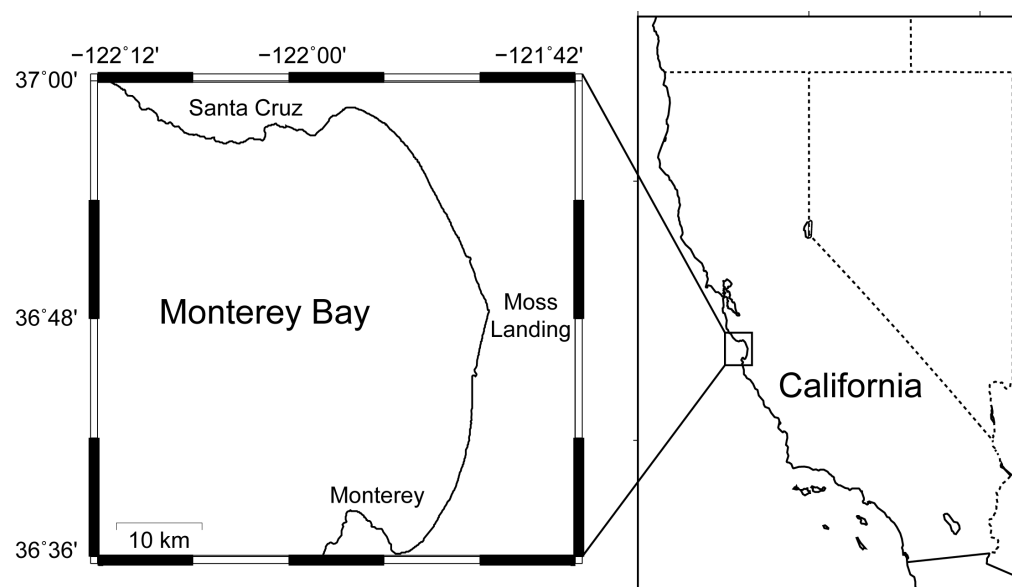


Fig. 3.1. Study Location. The Monterey Bay is a semi-enclosed bay along the central coast of California, USA.

1.4 Monterey Bay

The Monterey Bay, CA is an open bay located on the west coast of the USA, at the eastern fringe of the Northern California Current System (CCS), an eastern boundary current (Fig. 3.1). Its wind-driven circulation has been extensively described elsewhere [*Breaker and Broenkow, 1994; Pennington and Chavez, 2000*], but generally follows three oceanic seasons: upwelling (April – August), oceanic (September – October), and Davidson (November – March). This seasonal cycle is the climatological trend, though dates can vary and seasons can be interrupted with circulation consistent with other seasons. Typically during the upwelling season, recently upwelled water from just north of the bay is entrained into the bay where it bifurcates into a languid, northward flowing, cyclonic surface current and a southward flowing, anti-cyclonic surface current. The oceanic period is characterized by a relaxation of upwelling favorable winds, warming, and stratification of the surface ocean. The northern part of the bay, near Santa Cruz, lies in the wind shadow of the Santa Cruz Mountains [*J. P. Ryan et al., 2009*] and water temperatures here tend to be warmer than other regions of the bay. The Davidson period generally experiences downwelling favorable winds with episodic winter storm systems.

Patterns in phytoplankton ecology correspond to changes in physical and chemical conditions [*Smayda and Reynolds, 2001*] during these seasons. Diatoms tend to dominate during upwelling with its high nutrient flux and strong sheer-stress associated with vigorous mixing [*Smayda, 1997*]. During this period, some toxic

species of the diatom genus *Pseudonitzschia* produce domoic acid-- a neurotoxin that causes amnesiac shellfish poisoning and has caused extensive die-offs of marine mammals [*C A Scholin et al.*, 2000]. Dinoflagellates are sensitive to vigorous mixing and generally are not as abundant in Monterey Bay during the spring and summer. This slow growing group thrives in the nutrient-poor, stratified warm waters [Smayda, 1997] of the oceanic period. Dinoflagellates form extensive blooms in the northern Monterey Bay in a region termed the “red-tide incubator” [*J. P. Ryan et al.*, 2008]. Winds and prevailing water entrainment patterns concentrate dinoflagellates into this incubator [*J. P. Ryan et al.*, 2009]. Episodic wind reversals can result in mixed assemblages of diatoms and dinoflagellates [Fawcett et al., 2007]. In the Monterey Bay, it is not uncommon to find two co-dominant taxa either comingled within a surface bloom or in vertical layers with dinoflagellates in the nutrient-poor surface and a subsurface diatom bloom (personal observation).

The frequency and duration of these red-tide events have increased in recent years [*Jester et al.*, 2009]. The red-tide incubator of the northern part of the bay provides an excellent opportunity to study the physics supporting the blooms [*J.P. Ryan et al.*, 2005], the physiology of the various species that compose the blooms each year [*Kudela et al.*, 2008], the ecological succession of those species and their parasites [*Mazzillo et al.*, 2011], and the optics of the blooms. Some of these red-tide events have proved to be harmful to wildlife [*Jessup et al.*, 2009] and human health [*Honner et al.*, 2010] and are closely monitored.

One approach to monitoring is to identify and track algal taxa using optical signatures of the phytoplankton. Monitoring for HABs in Monterey Bay was one of the motivations for the algorithm developed in this study, though the algorithm has wider possible applications for modeling carbon flow in ecosystems and validating plankton functional type models. The objectives of this study were 1) to develop an optical signature library of phytoplankton taxa found in Monterey Bay, CA, 2) to develop a phytoplankton discrimination algorithm using the signature library, 3) to apply the algorithm to hyperspectral remote sensing reflectance spectra collected from a ship-board spectroradiometer and an airborne imager, and 4) to validate the algorithm using “synthetic” phytoplankton mixtures and field measurements of natural waters.

2.0 Methods

Nine large-scale cultures (Table 3.1) were grown for this study. The inherent optical properties of these cultures were measured and modeled. Because only six taxonomic groups were represented by the measured cultures, IOPs from other studies were also used [Dierssen *et al.*, 2006; Stramski and Kiefer, 1991]. The radiative transfer equations (RTE) (HydroLight™ V. 4.2; Sequoia Scientific, Inc.) computed remote sensing reflectance using the phytoplankton culture IOPs. These culture R_{rs} spectra formed the signature library. Unknown, natural water R_{rs} spectra from Monterey Bay were decomposed into constituent library components using the phytoplankton discriminator algorithm developed in this study. Biomass for each constituent was

computed and the model was validated using “synthetic” phytoplankton mixtures and independent species quantification measurements from the field. The study design is depicted schematically in Fig. 3.2.

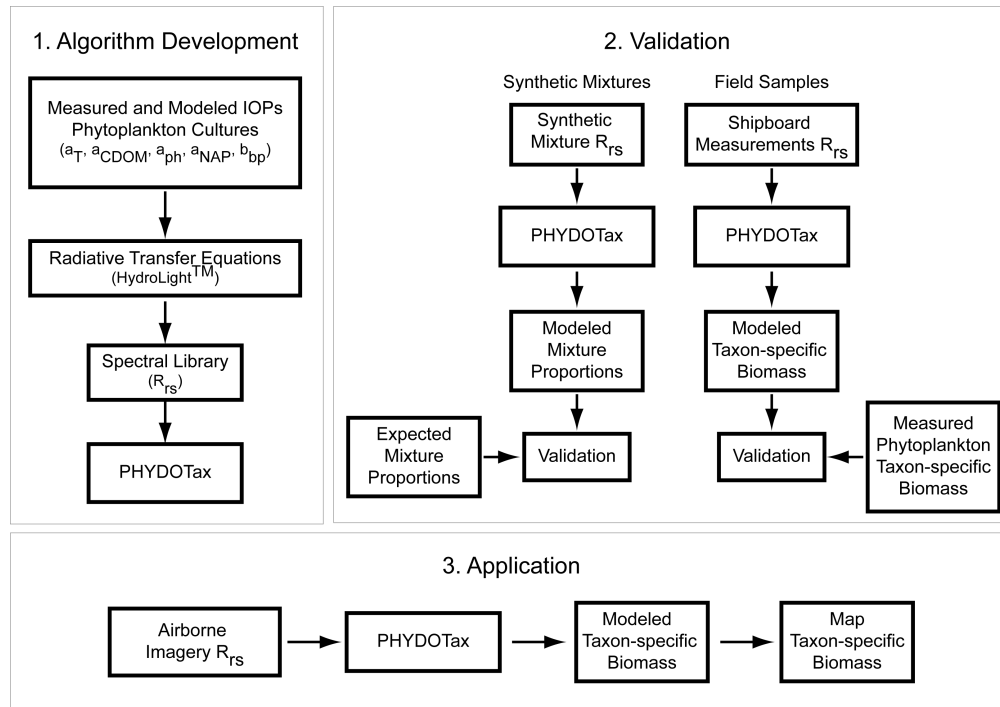


Fig. 3.2. Study Design. Schematic representation of the development, application, and validation of the phytoplankton discriminator, PHYDOTax.

2.1 Large-Scale Cultures

Nine phytoplankton cultures were grown to either 20 L or 200 L volumes. Genera selected included ones representative of the major color groups and those that could be cultured to a large volume. The nine phytoplankton genera included *Akashiwo*, *Amphidinium*, *Dunaliella*, *Isochrysis*, *Pseudonitzschia*, *Heterosigma*, *Skeletonema*, *Synechococcus*, and *Thalassiosira* (Table 3.1).

Table 3.1. Phytoplankton cultures used in the study.

Culture	Family	Group	Sample Date
<i>Akashiwo sanguinea</i>	Gymnodiniaceae	dinoflagellate	June 2, 2009
<i>Amphidinium carterae</i>	Gymnodiniaceae	dinoflagellate	February 16, 2007
<i>Dunaliella tertiolecta</i>	Chlorophyceae	chlorophyte	May 1, 2009
<i>Isochrysis galbana</i>	Isochrysidiaceae	haptophyte	April 23, 2009
<i>Pseudo-nitzschia</i> sp.	Bacillariaceae	diatom	May 1, 2007
<i>Heterosigma</i>	Heterosigmataceae	raphidophyte	October 24, 2007
<i>Skeletonema</i> sp.	Skeletonemaceae	diatom	December 3, 2008
<i>Synechococcus</i>	Synechococcaeeae	cyanobacteria	May 1, 2007
<i>Thalassiosira pseudonana</i>	Thalassiosiraceae	diatom	March 24, 2009
<i>Phycocyanin-rich Picoplankton</i>		UPCE	Stramski et al. 2001
<i>Emiliania huxleyi</i>	Noëlaerhabdaceae	haptophyte	Stramski et al. 2001
<i>Rhodomonas salina</i>	Pyrenomonadaceae	cryptophyte	unpub. data
<i>Prymnesium parvum</i>	Prymnesiophyceae	haptophyte	Stramski et al. 2001
<i>Pavlova lutheri</i>	Pavlovaceae	haptophyte	Stramski et al. 2001
<i>Porphyridium cruentum</i>	Porphyridiaceae	rhodophyte	Stramski et al. 2001
<i>Chroomonas fragarioides</i>	Chroomonadaceae	cryptophyte	Stramski et al. 2001
<i>Alexandrium catenella</i>	Goniodomataceae	dinoflagellate	unpub. data
<i>Ceratium</i> sp.	Ceratiaceae	dinoflagellate	unpub. data

The 200 L volume cultures included *Amphidinium*, *Pseudonitzschia*, *Heterosigma*, *Skeletonema*, and *Synechococcus*. The 20 L volume cultures consisted of *Akashiwo*, *Dunaliella*, *Isochrysis*, and *Thalassiosira*, grown in polycarbonate carboys. The 200 L culture chamber was a hard-bodied, translucent, cylindrical vessel measuring approximately 0.60 m in diameter and 1.0 m in height, lined with a translucent culture bag, aerated constantly with an aquarium bubbler, and loosely covered with a translucent lid to limit viral or bacterial contamination from the air circulation system in the environmental growth room. The seawater matrix for both the 20 L and 200 L

cultures was composed of InstantOcean™ artificial seawater amended with Guillard's f/2 culture media (Sigma-Aldrich Co.). The environmental growth room was maintained at 15°C ambient temperature and a 12:12 light cycle at ~ 100 μmol photons $\text{m}^{-2} \text{s}^{-1}$ (Sylvania "soft white" fluorescent lights). Growth rate was monitored with daily chlorophyll-*a* biomass measurements.

2.2 Sampling of Algal Cultures

Optical sampling commenced during late log-phase of algal growth. Discrete water samples were collected and filtered to measure chlorophyll-*a*, particulate light absorption (a_p), and light absorption by CDOM. A two-liter volume of the unfiltered culture sample was passed through a WETLabs, Inc. Spectral Absorption and Attenuation (ACS) light meter. The cultures grown to 200L were also sampled with a HOBI Labs HydroScat-6 backscattering sensor suspended directly into the growth chamber.

2.2.1 Filtered Culture Samples

Chlorophyll-*a* was measured fluorometrically following the EPA Method 445.0 [*Arar and Collins, 1997*] on a Turner Designs TD-700 fluorometer and concentration was calculated using the calibration coefficient for the particular fluorometer (calibrated annually). Optical density (OD) of particles and CDOM was measured on a Cary UV-Vis Spectrophotometer (300 – 800 nm, with 0.5 nm resolution). Light absorption by algal and non-algal particles was measured by filtering an aliquot of sample (in

triplicate) onto a glass fiber filter (GF/F; Whatman®) using a low pressure vacuum. Sample and MilliQ-water blank filters were immediately scanned on the spectrophotometer for OD of total particles, then bleached with a 1.52 M NaClO solution, and re-run on the spectrophotometer to derive the algal- and non-algal particle contributions to total particulate absorption. The MilliQ blank was subtracted from the sample OD. The particulate absorption coefficient was calculated using Equation 6:

$$a_p(\lambda) = \frac{2.303 * OD_{(\lambda - \lambda_{750})}}{V/A_{\text{pad}}} \quad (6)$$

Where 2.303 is the correction factor for the natural log transform, V is volume filtered, and A_{pad} is the area of the filter-pad. The multiple scattering effects of the glass fiber filters were subtracted following the protocol of Cleveland and Weidemann [Cleveland and Weidemann, 1993]. The absorption coefficient of non-algal particles, $a_{\text{NAP}}(\lambda)$, the bleached scan, was subtracted from the total absorption coefficient, $a_p(\lambda)$, to obtain the absorption coefficient for phytoplankton, $a_{\text{ph}}(\lambda)$. Biomass normalized light absorption was calculated by dividing $a_{\text{ph}}(\lambda)$ by the chlorophyll-a concentration of the culture sample. The absorption coefficient of CDOM was measured by filtering a volume of culture through a 0.2 µm Nuclepore® polycarbonate filter and then scanning the filtrate immediately on the spectrophotometer using a 0.1m pathlength quartz cuvette. A MilliQ-water blank was

subtracted from these values and the absorption coefficient was calculated using Equation 7:

$$a_{CDOM} = \frac{2.303 * OD_{(\lambda - \lambda 750)}}{0.1} \quad (7)$$

The total absorption coefficient was determined by adding the absorption coefficients for particles, CDOM, and published values for pure water (Pope and Fry 1997).

2.2.2 Optical Instrument Sampling

2.2.2.1 Spectral absorption and attenuation data collection and processing

The total absorption and attenuation coefficients of the cultures were measured using a hyper-spectral absorption and attenuation (ACS) meter manufactured by WETLabs, Inc. The ACS features two rigid flow-through tubes through which water is pulled, with the pump upstream of the sensor. Light emitting and detecting sensors measure total absorption and attenuation. For the benchtop set-up for this study, the flow configuration was altered from the standard field set-up to assure bubble-free sampling. Instead of the field deployed Seabird T5 pump, a large volume peristaltic pump (ColeParmer, Inc.) was placed upstream of the flow tubes and water was drawn successively through each rigid tube via flexible tubing for approximately one minute. Data were captured every 250 ms on a nearby PC-laptop running WetView 7.1 (WETLabs, Inc.). Care was taken to collect at least 10 consecutive seconds of bubble-free spectra. Clean-water calibrations were collected prior to each culture

sampling to evaluate instrument drift over the course of the study. Drift was negligible.

The culture biomass for *Amphidinium*, *Synechococcus*, and *Thalassiosira* exceeded the sensitivity of the attenuation sensor. Attenuation values for these cultures were modeled by fitting a sixth order polynomial to the known attenuation spectra for cultures that were within the sensor range. A least-squares fit was applied to the roots of the polynomial to absorption at 673 nm (the chlorophyll-*a* peak). New attenuation spectra were reconstructed for the three cultures. Attenuation was estimated for these cultures by modeling chlorophyll-specific attenuation for the other cultures and deriving spectral attenuation for the unknown samples by using the linear relationship of the known samples at each sensor wavelength (C. Mobley, pers. comm.).

2.2.2.2 Backscattering data collection and processing

The HydroScat-6, HS6, (HOBILabs, Inc.) is a field deployable instrument that measures optical backscattering at six independent wavelengths and one acceptance angle (140°). It also measures fluorescence at two wavelengths, one of which is for chlorophyll-*a* biomass. The measurement is converted to volume scattering function at 140° and that value is converted to backscattering. A sigma correction is applied to account for light lost due to attenuation between the sample material and the sensor (HS6 Manual). These sigma-corrected values were used in this study to obtain optical backscattering over the visible range.

The particular instrument used during this study measured backscattering at the wavelengths; 442 nm, 488 nm, 532 nm, 589 nm, 620 nm, and 671 nm prior to 2008, and then was refurbished and new diodes and sensors were installed which measured backscattering at 420 nm, 442 nm, 470 nm, 510 nm, 590 nm, and 700 nm. The magnitude and spectral shape for each culture were of interest, not a single measurement at a particular wavelength, so this change in detection wavelengths was not problematic.

Because of the geometry of the optical diodes and sensors, sampling small culture volumes (< 200 L) was not recommended due to optical contamination by the sides and bottom of the culture container, and backscattering was measured directly in the culture chamber for the 200 L cultures only. The aquarium bubbler was turned off at least 10 minutes before sampling. The lid was removed and the bag liner adjusted so it was directly against the container walls. The culture was gently “stirred” with a MilliQ-rinsed plastic paddle. The instrument was powered and the face was carefully lowered into the culture at a 45° angle and then positioned horizontally to face downward in the culture; this reduced the likelihood of bubbles adhering to the sensor windows. The instrument face was positioned 15 cm below the surface of the culture and 45 cm above the bottom of the culture chamber. Care was taken to keep the instrument centered in the culture chamber to prevent optical contamination from the sides of the container. Data were collected each second for a minimum of three minutes, stored to internal memory and then uploaded, with calibrations and corrections applied, using HydroSoft (HOBILabs, Inc.). Suspect data

were flagged and deleted. Reliable spectra were loaded into MATLAB (The Mathworks, Inc) and converted to text files formatted for HydroLight™. These data, and the total absorption and attenuation data from the whole water samples and ACS, were used as inputs to compute remote sensing reflectance. Backscattering for the other cultures grown only to 20 L was modeled using HydroLight™.

Particulate backscattering was modeled for the published phytoplankton cultures and the smaller volume cultures grown for this study. Backscattering values were modeled with HydroLight™ using the case 2 method where IOPs were obtained from a 4-component model for case 2 waters. Minerals and CDOM were held at zero and only the contribution to backscattering due to phytoplankton was estimated. Output wavelengths corresponded with the HS6 wavelengths. Initially, this method was performed on the absorption and attenuation properties of the five large volume cultures as a test to see if HydroLight™ could approximate the correct b_{bp} . The method was repeated six times for each culture to test six scattering phase functions in order to find the best fit between modeled and measured b_{bp} . The FFbb016 discretized phase function had the best fit (data not shown). So b_{bp} was modeled for the other library taxa using this input parameter in HydroLight™.

2.3 Modeling $R_{rs}(\lambda)$

Remote sensing reflectance for the phytoplankton cultures was computed using the radiative transfer equations (RTE) to estimate the radiance distribution within an idealized, mono-specific water column. HydroLight™ solves the RTE with user-

supplied data and sub-routines. Table 3.2 summarizes the HydroLight™ simulation input parameters used for each culture. Generally, user supplied inputs included light absorption by phytoplankton and CDOM; total absorption and attenuation measured with the ACS; published values for absorption and backscattering by water [*Pope and Fry, 1997*]; and particulate backscattering. In some instances the inputs for absorption, attenuation, or b_{bp} were modeled from complimentary measurements and then applied to the RTE as ‘user-supplied’ inputs to HydroLight™. Seven combinations of sun angle, wind speed, and cloud cover were modeled for each culture to approximate the conditions most likely encountered in the field. The air-water surface boundary conditions were set to 0 or 5 m s⁻¹ wind speed and a semi-empirical sky model based on RADTRAN. Sky conditions were set to 0, 20, 30, or 45° sun angle and either 0 or 20% cloud cover. The angular pattern for sky radiance was modeled with the hcnnrad function within HydroLight™. An infinitely deep bottom-boundary condition was established and the RTE were solved at 1 nm resolution for the upper 1.5 m of the idealized water column. Biomass-normalized Rrs ($R_{rs\ norm}$) was computed by dividing Rrs by its value at 673 nm. Rrs norm was binned to 5 nm resolution for use in the signature library. Only the surface $R_{rs\ norm}$ spectra were used for the signature library.

Table 3.2. Input parameters used for radiative transfer equations to simulate remote sensing reflectance spectra from pure phytoplankton cultures. 'X' denotes measured parameter.

Culture	a_{ph}	a_{CDOM}	ACS - a	ACS - c	HS6 - b_b	Sun Angle (degrees)	Wind Speed ($m s^{-1}$)	Cloud Cover (%)
<i>Akashiwo sanguinea</i>	X	X	X	X	modeled	0, 20, 30, 45	0, 5	0, 20
<i>Alexandrium</i>	X	X	modeled	modeled	modeled	0, 20, 30, 45	0, 5	0, 20
<i>Ceratium</i>	X	X	modeled	modeled	modeled	0, 20, 30, 45	0, 5	0, 20
<i>Dunaliella tertiolecta</i>	X	X	X	X	modeled	0, 20, 30, 45	0, 5	0, 20
<i>Emyliana huxleyii</i>	X	X	modeled	modeled	modeled	0, 20, 30, 45	0, 5	0, 20
<i>Pavlova lutheri</i>	X	X	modeled	modeled	modeled	0, 20, 30, 45	0, 5	0, 20
<i>Prymnesium parvum</i>	X	X	modeled	modeled	modeled	0, 20, 30, 45	0, 5	0, 20
<i>Pseudo-nitzschia sp.</i>	X	X	X	X	X	0, 20, 30, 45	0, 5	0, 20
<i>Porphyridium cruentum</i>	X	X	modeled	modeled	modeled	0, 20, 30, 45	0, 5	0, 20
<i>Heterosigma</i>	X	X	X	X	X	0, 20, 30, 45	0, 5	0, 20
<i>Rhodomonas salina</i>	X	X	modeled	modeled	modeled	0, 20, 30, 45	0, 5	0, 20
<i>Skeletonema sp.</i>	X	X	X	X	X	0, 20, 30, 45	0, 5	0, 20
<i>Synnechococcus</i>	X	X	X	modeled	X	0, 20, 30, 45	0, 5	0, 20
<i>Thalassiosira pseudonana</i>	X	X	X	modeled	modeled	0, 20, 30, 45	0, 5	0, 20
UPCE	X	X	modeled	modeled	modeled	0, 20, 30, 45	0, 5	0, 20

2.4 Field Study

The field study was conducted in the Monterey Bay (Fig. 3.1), an open bay along the central California, USA coast. Data collection occurred during four cruises aboard the *R/V John H. Martin* in September 2006, October 2008, October 2009, and October 2010. *In situ* optical and whole water sampling occurred inside and outside of red-tide patches, primarily in the central and north-east sections of the bay. The underway data acquisition system on the boat recorded temperature, salinity, and chlorophyll-*a* fluorescence. For the 2006, 2008, and 2010 cruises, a mini-rosette, equipped with a Seabird SBE 19plus CTD, WetStar fluorometer (WETLabs, Inc), and ten 1.5 L Niskin bottles sampled from the water column at each station. A 5 L Niskin bottle deployed to 5 m and a bucket sample from the surface were used to collect water samples in 2009. Discrete water samples were collected to measure chlorophyll-*a*, particulate light absorption, light absorption by CDOM, pigments (2006), and a suite of other biologically relevant data not used in this study. Following water collection, hyper-spectral absorption and attenuation (ACS, WETLabs, Inc) and optical backscattering (HS6, HOBI Labs, Inc.) were collected. At the same time, hyper-spectral downwelling irradiance (E_d) and upwelling radiance (L_u) (350 – 800 nm; 0.3 nm resolution) were measured with the Satlantic HyperPro II profiling spectral radiometer in “floater” mode (HyperTSRB-Profiler II, Satlantic, Inc). Surface and profiling measurements were collected with the instrument in both floater and profiling mode. The HyperTSRB-Profiler II data were processed using ProSoft 7.7.12 to Level 3 and then remote sensing reflectance was computed from L_u and E_d

using MATLAB. Surface R_{rs} was normalized to the passive-fluorescence peak at a wavelength higher than 673 nm to derive a biomass normalized, remote sensing reflectance spectrum. Only surface $R_{rs\ norm}$ was used in this study.

In 2006, phytoplankton identification and cell enumeration were performed on water samples using the Flow CytoBot [Olson and Sosik, 2007; Sosik and Olson, 2007]. Cell area per milliliter ($\mu\text{m mL}^{-1}$) was measured for every chlorophyll-*a* containing cell and then grouped into genus or photosynthetic group. A total of nine major groups were observed: dinoflagellates, diatoms, haptophytes, chlorophytes, unspecified chlorophyll-containing, cryptophytes, chrysophytes, silicoflagellates, and “round cell” which was a mixture of chlorophytes, cryptophytes, and haptophytes. The “round cell” group was divided into thirds and each third was applied to chlorophytes, cryptophytes, and haptophytes. The total area of cells was computed for the taxonomic groups (dinoflagellates, diatoms, haptophytes, chlorophytes, cryptophytes, unspecified picoeukaryotes, chrysophytes, and silicoflagellates) and the proportion of each was computed by dividing the group area by the total area. The proportion was then multiplied times the total chlorophyll-*a* concentration to derive the measured taxon-specific biomass used in validation (Equation 8).

$$B_{\text{taxon}} = \frac{A_{\text{taxon}}}{\sum A_{\text{taxon}}} * [chl - a] \quad (8)$$

Where B_{taxon} is taxon-specific biomass from measured samples, A_{taxon} is the area per mL measured for a particular taxon, and [chl-a] is measured chlorophyll-*a* concentration. Chrysophytes and silicoflagellates were not used in the validation because the algal discriminator did not include those taxa in the signature library. Cyanophytes were not detected with the Flow CytoBot. Instead, the ratio of the pigment zeaxanthin to chlorophyll-*a* was used as a marker for the cyanobacterium *Synechococcus* [Kana et al., 1988].

2.5 Hyperspectral Imagery

Details of image collection can be found elsewhere [Davis and Bissett, 2007], but the salient points are summarized here. Hyper-spectral overflight imagery was collected as a part of the Coastal Ocean Applications and Science Team (COAST) cruise from September 3 – 15, 2006 in Monterey Bay, CA. COAST was formed by the National Oceanographic and Atmospheric Administration (NOAA) to develop ocean color algorithms for the next Geo-stationary Operational Environmental Satellite (GOES-R). Imagery was collected on four days during this period using the Spectroscopic Aerial Mapper with On-board Navigation (SAMSON, Florida Environmental Research Institute). SAMSON was mounted inside of a Twin Otter aircraft and collected hyper-spectral imagery covering 256 bands in the UV to NIR range (3.5 nm resolution over 380 to 970 nm) with 5 m spatial resolution. Overflights covered a grid in the north-east part of the bay in a region that could be completed in 30 minutes, and then re-sampled for a five-hour duration. The time series was intended to capture

the surface expression of vertically migrating dinoflagellates present in an extensive red-tide that coincided with the research cruise. Imagery data were calibrated, geolocated, and atmospherically corrected. The best image available (10 am local time; September 12, 2006) was downloaded from the server, imported into ENVI (ITT, Inc.) where a land and kelp forest mask was applied to the scene and a correction factor (1×10^{-6}) was applied to obtain the accurate scale for remote sensing reflectance (D. Kohler, pers. comm.). The imagery had a spectral resolution of 5 nm at 10 m spatial resolution. Data were then exported to ASCII and imported into MATLAB to estimate chlorophyll-*a* biomass and for further analysis with the phytoplankton discriminator algorithm.

Chlorophyll-*a* biomass was estimated from fluorescence line height (FLH) [Abbott and Letelier, 2006]. A linear regression of ship-board measured FLH was fit to chlorophyll-*a* measurements from water samples for the 2006 research cruise. This relationship ($y = 6.65 * 10^4 (\text{FLH}) - 37.7$; $r^2 = 0.94$, $p < 0.05$) was then used to compute chlorophyll-*a* concentration from imagery FLH.

2.6 Phytoplankton Discriminator Algorithm

The phytoplankton taxon discrimination algorithm employs similar techniques as CHEMTAX [Mackey *et al.*, 1996], an algal discriminator based on phytoplankton pigment absorption. The algorithm uses phytoplankton detection with optics to discriminate to algal taxon, hence its name: PHYDOTax. The algorithm is composed of three steps. The first step uses matrix algebra to decompose a measured, or

unknown, $R_{rs\ norm}$ spectrum into its constituent parts represented in a signature library, developed from phytoplankton culture measurements. The signature library matrix, S, is a subset of the culture library $R_{rs\ norm}$ at 10 nm increments from 455 nm to 675 nm. The unknown vector, u, is a subset of $R_{rs\ norm}$ at 10nm increments from 455 nm to 675 nm for each unknown sample (i.e. culture mixtures, *in situ* R_{rs} measurements from shipboard instruments, or $R_{rs\ norm}$ spectra from imagery). The algorithm can be described as the solution for a vector of coefficients, m, in the following equation (Equation 9):

$$u = S \bullet m \quad (9)$$

Which, when re-arranged to solve for m is the solution to the dot product of the inverse-matrix of the signature library, S, and the unknown spectrum, u:

$$m = S^{-1} \bullet u \quad (10)$$

Because S is a non-square matrix (i.e. more $R_{rs\ norm}$ measurements than taxon categories being solved), the pseudo-inverse of S is used instead. The solution is a best-fit approach using a least squares minimization technique. Using the pseudo-inverse of S, a more accurate representation of Equation 10 is (Equation 11):

$$m = S^+ \bullet u \quad (11)$$

where $+$ represents the pseudo-inverse (note: $+$ is not to be mistaken for ‘T’). As this is an over-determined solution, the number of wavelengths used in the signature library must exceed the number of taxa being resolved.

For the second step, the result of the dot product is used to compute the proportion of each signature taxon within the unknown (Equation 12):

$$\text{Proportion} = \frac{X_{\text{unknown}}}{\sum X_{\text{unknown}}} \quad (12)$$

In the third step, this proportion is then multiplied times the total chlorophyll-*a* biomass to arrive at taxon-specific biomass present within the unknown sample.

2.7 Validation

PHYDOTax was first validated using “synthetic” mixtures of the culture library. These synthetic mixtures were simply the mathematical addition of library $R_{rs \text{ norm}}$ spectra that were then re-normalized by the biomass peak. Two-, three-, five-, six-, and seven- taxon combinations were computed using this method for a total of 158 possible synthetic mixtures. A Wilcoxon rank-sum test was used to evaluate if the model predictions for phytoplankton proportion computed from PHYDOTax fit the expected proportions. The non-parametric Wilcoxon rank sum test was selected instead of the Chi-square goodness-of-fit because proportions were being compared, and because the expected proportions were would not have met the assumption of a

normal distribution of values [Zar, 1996]. A critical p-value of 0.05 was used to evaluate significance.

The second validation was conducted on field measurements collected in 2006 and 2010. Validation tested the null hypothesis that there was no difference in taxon-specific biomass between measured and modeled estimates. A paired t-test (critical p-value = 0.05) was used to test the hypothesis. Thirteen surface stations from 2006 and five from 2010 had both model predictions and cell enumeration data. Additionally, a test of linear regression was performed on these biomass estimates to determine the goodness-of-fit. Of these thirteen validation stations in 2006, only eleven had pigment measurements. Zeaxanthin concentrations ranged between 0 and 0.26 mg m⁻³ for all stations. Zeaxanthin to chlorophyll-*a* ratios were essentially 0 mg m⁻³ for seven of those stations, 0.01 mg m⁻³ for three stations, and 0.03 mg m⁻³ for one station. These ratios were so low as to be considered evidence of no cyanophytes in the samples [Kana *et al.*, 1988]. PHYDOTax predicted zero biomass for cyanophytes in all but one station (M006 at 1.18 mg m⁻³). Because of these numerous zero-values, it was not possible to perform statistics comparing measured and modeled taxon-specific biomass, other than to note a 91% agreement in zero biomass.

3.0 Results

3.1 Library Development

The total light absorption coefficient of algal cultures used in this study, both measured and from published values, is presented in Figure 3.3. The absorption

spectra of dinoflagellates, diatoms, raphidophyte, cryptophytes, and haptophytes share similar shape due to pigment composition (Fig. 3.3A & 3.3B). Cyanophytes and chlorophytes share a similar shape with cyanophytes having a distinct peak at 620 nm (Fig. 3.3C). Rhodophytes and UPCE (Fig. 3.3D) share similar pigments and also spectral shape. Of the algal cultures, five reside in the “brown” color group defined by Beutler et al. 2002 [Beutler *et al.*, 2002]. Therefore, distinguishing among them solely on the basis of absorption properties is inconclusive. Of note are the absorption spectra of the cyanophyte, rhodophyte, and unidentified pycocyanin-rich picoeukaryotes (UPCE). These taxa have distinguishing absorption peaks at 550 nm and at 625 nm (Fig 3.1B) related to the phycobili-protein pigments present. These taxa can be resolved from the brown group based on absorption properties (analysis not shown).

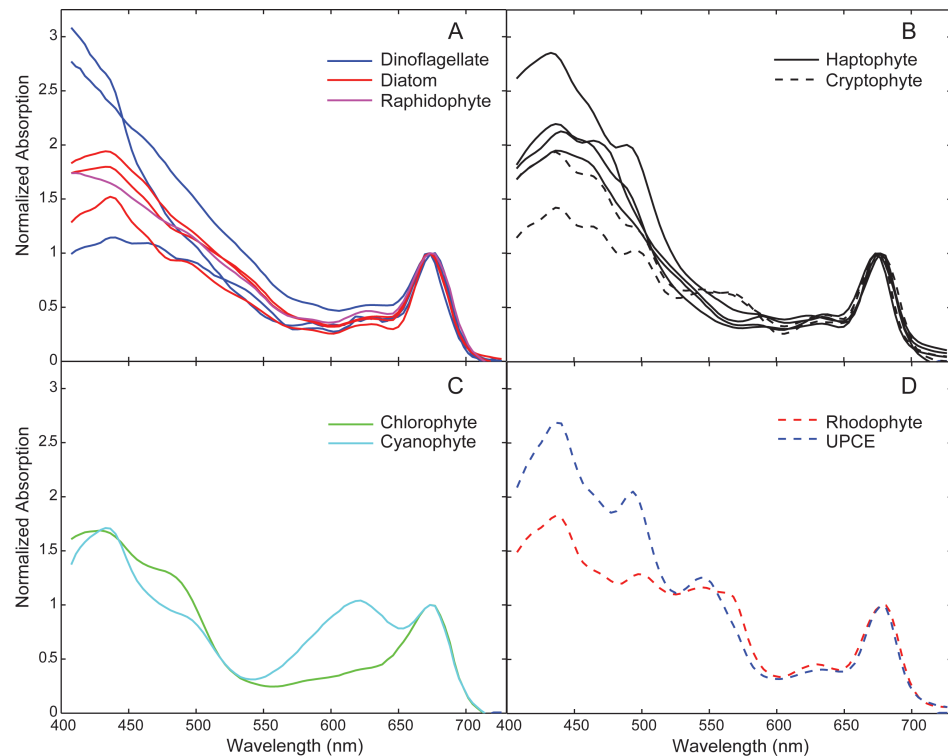


Fig. 3.3. Absorption Coefficient – cultures. Total absorption coefficient of phytoplankton cultures. Spectra measured using the WetLabs, Inc. ACS and processed according to Methods, spectra normalized to peak value at 673 nm. (A) dinoflagellates, diatoms, and raphidophytes, (B) haptophytes and cryptophytes, (C) chlorophytes and cyanophytes, (D) rhodophytes and unspecified phycocyanin containing pico-eukaryotes – UPCE.

Figure 3.4 presents the backscattering coefficient of some representative algal cultures used in this study. Variation in bio-volume, cell wall material, and cell concentration can result in differences in backscattering magnitude and shape. For example, chlorophytes (green) and UPCE (blue dashed) had higher backscattering than the diatoms (red) and dinoflagellates (blue solid), which have a larger bio-volume. This is a pattern consistent with observations and optical principles.

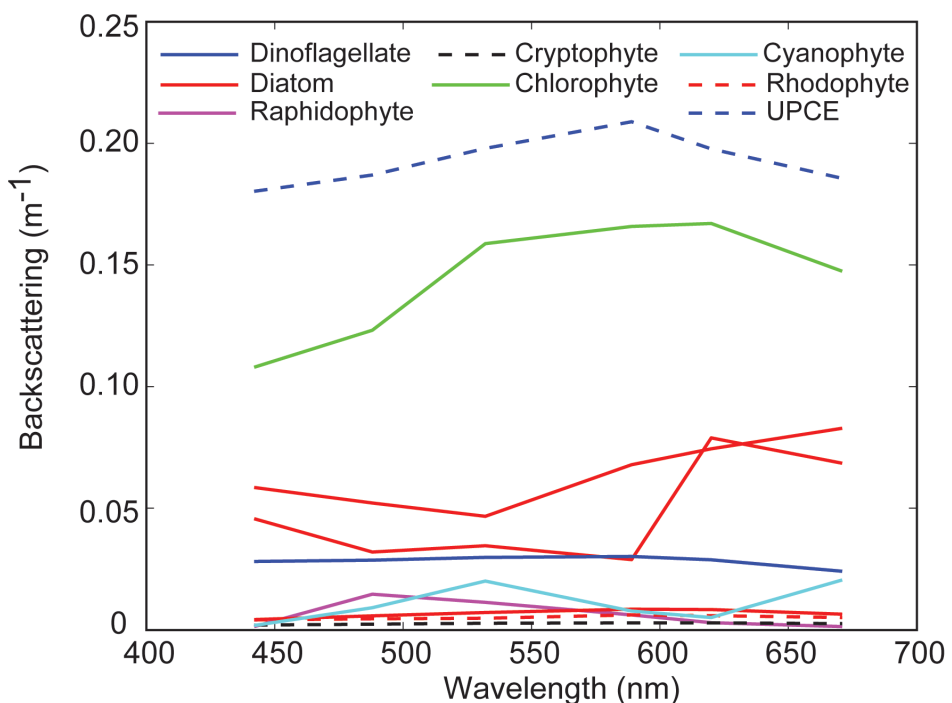


Fig. 3.4. Backscattering Coefficient – cultures. Total backscattering coefficient, measured and modeled, for some representative algal taxa.

The mean normalized R_{rs} spectra for the library taxa are presented in Figure 3.5. Dinoflagellates, diatoms, raphidophytes, and haptophytes shared similar spectral shape and magnitude (Fig. 3.5A). Dinoflagellates and diatom spectra varied slightly in the peak wavelength and complexity in spectral shape at the shoulder from 550 nm to 650 nm. A large spectral peak between 500 nm and 600 nm, relative to biomass, characterized haptophytes (Fig. 3.5B). Cryptophytes had no dominant peak, but instead had multiple smaller peaks (Fig. 3.5B). The spectral shape of chlorophytes followed a relatively simple shape, as expected from its pigment composition, and had a peak between 525 nm and 600 nm that was approximately equal in magnitude to the biomass peak (Fig. 3.5C). Cyanophytes had a distinctively low peak height in the 525 nm to 575 nm range relative to the biomass peak (Fig. 3.5C). Rhodophytes differed from all other taxa with a prominent peak shifted further into the red (600 nm) with several lesser peaks between 490 nm and 540 nm (Fig. 3.5D). Because rhodophytes and raphidophytes compose such a small portion of the species assemblage in the Monterey Bay, they were eliminated from the spectral library for this study.

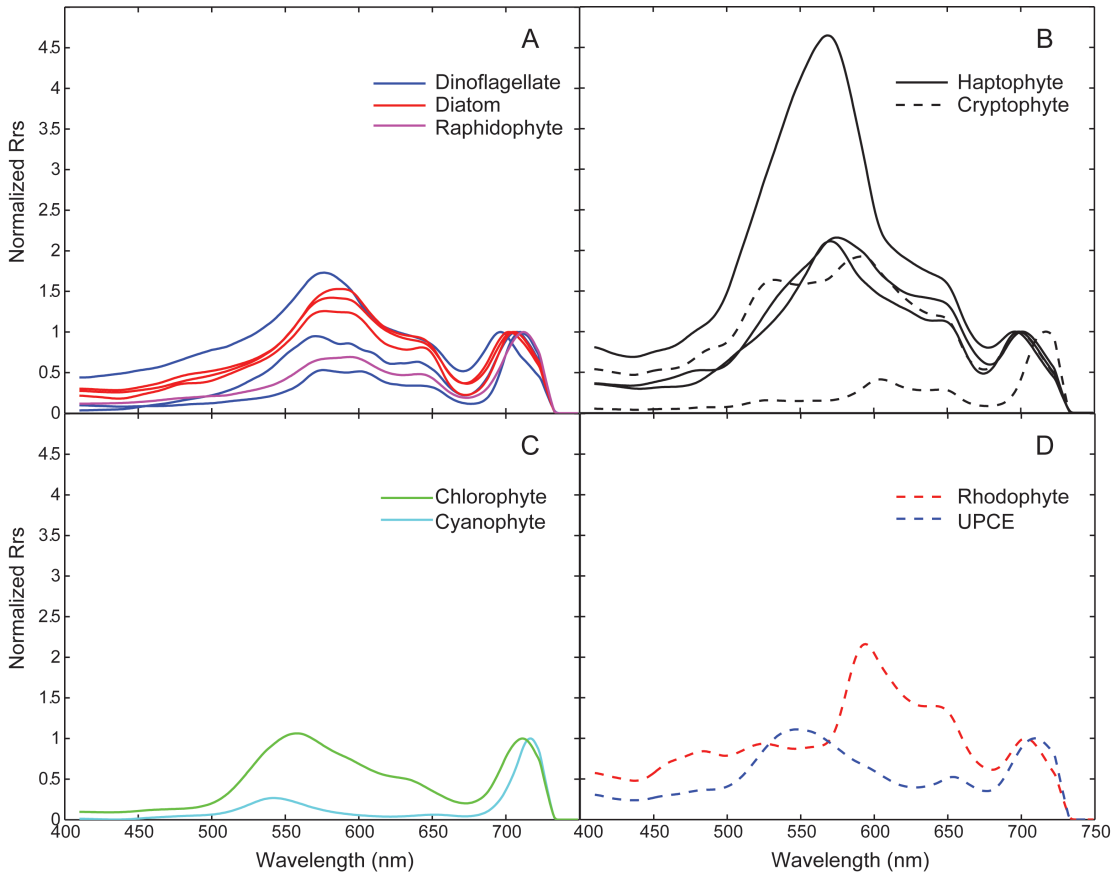


Fig. 3.5. Modeled Remote Sensing Reflectance (Rrs) - cultures. Rrs spectra of algal cultures, computed using radiative transfer equations, according to Methods, spectra normalized to peak value greater than 680 nm to derive ‘biomass’ normalized Rrs. (A) dinoflagellates, diatoms, and raphidophytes, (B) haptophytes and cryptophytes, (C) chlorophytes and cyanophytes, (D) rhodophytes and UPCE.

3.2 *In situ* Field Predictions

The field stations from each of the four research cruises are presented in Fig. 3.6. Station location was selected to sample both red-tide bloom and non-bloom waters in all years. Stations were distributed throughout the northern part of Monterey Bay in 2006. Sampling in 2008 was mostly in the northern part of the bay with some sampling just south of Moss Landing, CA in order to collect spectra from a filament of red-tide water in that region. The cluster of stations near Moss Landing is from an eight-hour time series within a dinoflagellate –dominated red-tide ($\sim 30 \text{ mg chl m}^{-3}$). Sampling in 2009 and 2010 was also distributed throughout the northern part of the bay. Only a subset of stations are represented in the figure in which both whole water and optical measurements were available.

Normalized remote sensing reflectance spectra for each station represented in Fig. 3.6, is presented in Fig. 3.7. The spectral shape and magnitude vary among stations within and among years as would be expected from the diverse water masses sampled (red-tide patch, river plume, non-bloom waters). Generally, there is a prominent peak between 550 nm and 620 nm. In some spectra, the magnitude of R_{rs} norm was high from 400 nm to 550 nm, relative to the peak. This was likely due to the contribution of small scattering particles. These spectra in Fig. 3.7 were the ship-board measurements of hyperspectral R_{rsnorm} used to model taxon-specific biomass with PHYDOTax.

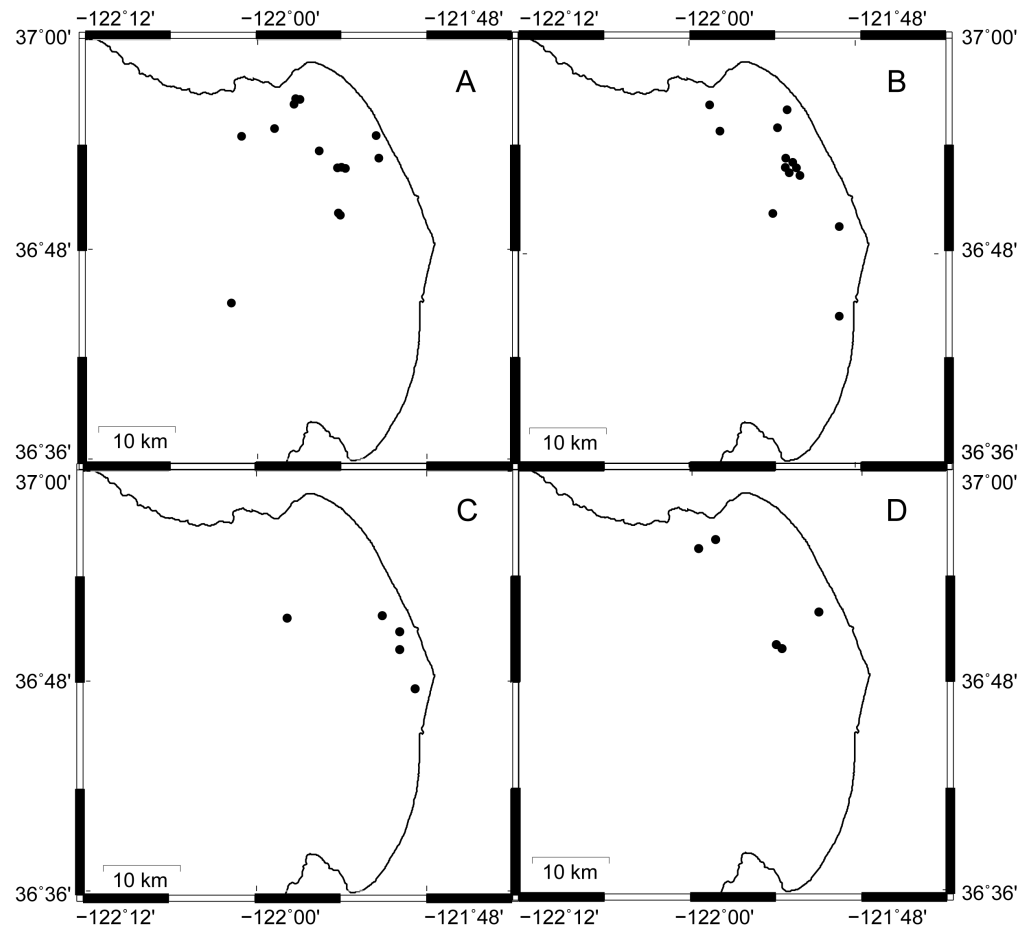


Fig. 3.6. Study Stations. Study stations for each research cruise during the four-year program. (A) COAST - 2006, (B) MB08 – 2008, (C) MB09 – 2009, (D) MB10 – 2010.

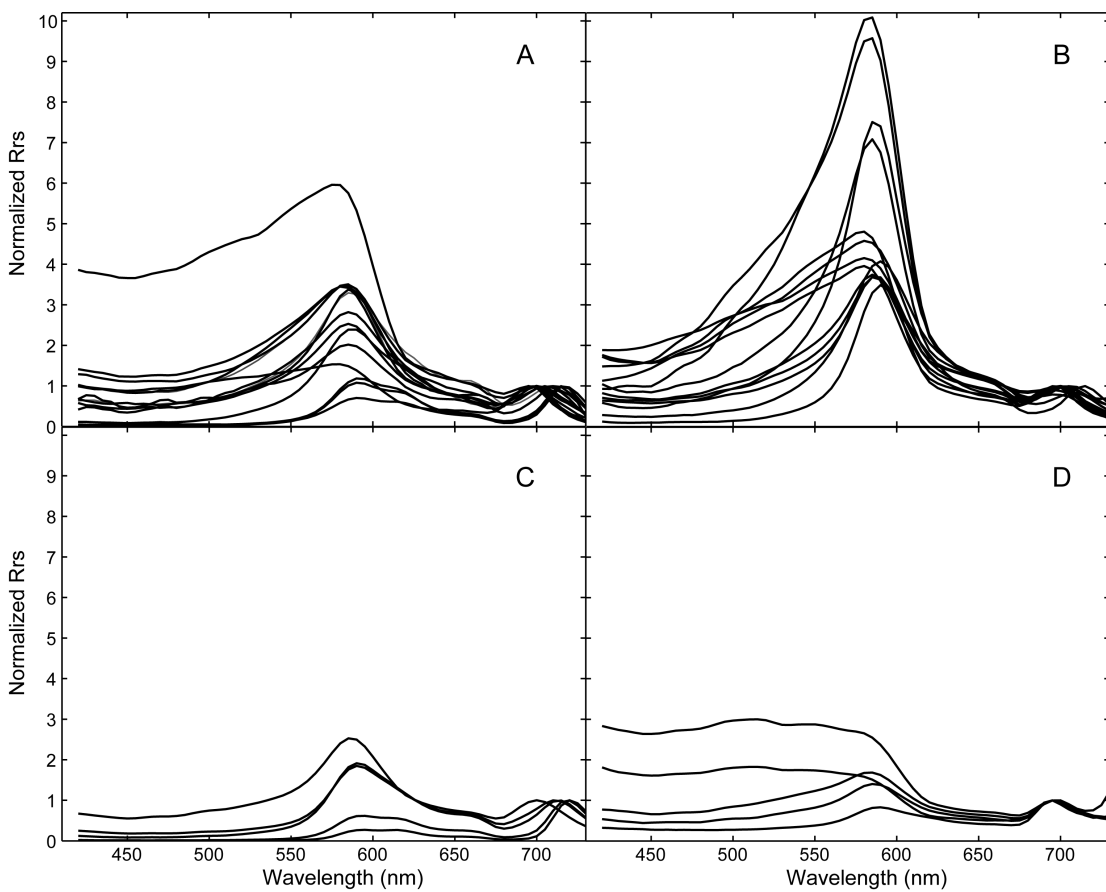


Fig. 3.7. In situ Rrs – field samples. Measured surface remote sensing reflectance, normalized by the maximum peak value greater than 673 nm, from the four research cruises (A) COAST - 2006, (B) MB08 - 2008, (C) MB09 - 2009, and (D) MB10 - 2010. Rrs was measured *in situ* using a Satlantic HyperPro Profiler II. Only surface samples were used in this study.

PHYDOTax predictions for taxon-specific biomass in 2006 are presented in Table 3.3. Measured chlorophyll-*a* concentration was higher than the typical concentration (5 mg m⁻³) found during September in the Monterey Bay [Pennington and Chavez, 2000]. In fact, chlorophyll-*a* concentration was above typical levels at all stations in the bay ranging from 5.7 to 332 mg m⁻³. PHYDOTax predicted that dinoflagellates dominated the biomass at several stations, sometimes reaching 70% of the total in 2006. At other stations, however, PHYDOTax predicted fairly evenly mixed assemblages of dinoflagellates and diatoms. Within the red-tide, PHYDOTax predicted relatively high concentrations of diatom biomass ranging from 0 to 101 mg m⁻³. Haptophytes were predicted to have relatively low biomass, possibly due to the season. Chlorophytes, UPCE, and cryptophytes were predicted to be present in low concentrations. Trace levels of cyanophytes were predicted for all shipboard measurements, with the exception of the offshore M1 station where cyanophytes were predicted to occupy 15% of the taxon assemblage. Dinoflagellates were predicted to have had high chlorophyll-*a* concentrations in the northern part of the bay, intermingled with diatoms. The stations with the predicted concentrations of high diatom biomass were isolated to one part of the bay, inshore of the usual location of the red tide incubator, near Aptos, CA.

Table 3.3. COAST 2006. Taxon-specific biomass estimates from PHYDOTax for Rrs collected from the ship in September 2006.

Station	Date	Lat	Lon	Measured [chl-a] (mg m- 3)	Predicted Chlorophyll Concentration by Taxonomic Group						
					Dino	Diatom	Hapt	Chloro	Cyano	UPCE	Crypto
M002	9/5/06	36.8776	-121.8971	7.8	5.64	1.28	0.55	0.34	0	0	0
M003	9/5/06	36.9385	-121.9543	40.0	17.50	5.64	2.34	7.85	0	6.67	0
M004	9/5/06	36.8782	-121.9023	14.0	7.52	2.61	1.00	1.18	0	0.86	0.83
M005	9/6/06	36.8785	-121.8980	8.0	5.72	1.24	0.36	0.61	0	0	0.08
M006	9/6/06	36.8778	-121.8948	8.0	2.35	4.30	0.13	0.05	1.18	0	0
M007	9/7/06	36.8876	-121.8550	300.0	140.47	101.53	6.21	26.91	0	24.88	0
M008	9/8/06	36.8341	-121.9009	25.0	14.26	5.71	1.02	0.40	0	1.50	2.09
M009	9/8/06	36.7497	-122.0291	8.0	6.31	0	0.17	0.09	0	0	1.43
M011	9/11/06	36.8951	-121.9248	50.0	32.80	7.48	1.88	3.14	0	4.71	0
M012	9/11/06	36.9087	-121.8582	332.0	170.15	89.75	9.19	22.01	0	40.90	0
M013	9/12/06	36.9082	-122.0161	5.7	3.99	0.84	0.19	0.68	0	0.00	0
M014	9/12/06	36.8354	-121.9036	39.0	18.16	6.84	1.60	5.07	0	7.32	0
M015	9/12/06	36.9154	-121.9770	119.0	63.65	34.65	3.63	6.69	0	10.37	0
M016	9/15/06	36.9430	-121.9489	32.0	12.38	11.38	3.24	2.74	0	2.26	0
M017	9/15/06	36.9437	-121.9519	35.0	18.87	7.72	1.04	3.46	0	3.91	0

Monterey Bay experienced a less intense and patchier red-tide in 2008 than in 2006 (Table 3.4). Measured chlorophyll-*a* concentrations ranged from 3.8 to 30 mg m⁻³. PHYDOTax predicted that the bloom was dominated by dinoflagellates, but only slightly more than diatoms in most cases at 30 to 50% of the biomass. One exception was a station at the Salinas River mouth south of Moss Landing where diatoms represented 52% of the taxon assemblage. Predicted concentrations of all other phytoplankton taxa were very low for 2008. The red-tide existed in sparse filaments oriented north to south from the northern part of the bay off of Aptos, CA towards Moss Landing, CA and then southward to Marina, CA. One of these patches located just offshore of Moss Landing, CA was intensively sampled for an 8-hour time series beginning at 10 am and ending at 6 pm local time on October 17, 2008. Only five hours of data were used in which sun angle produced reliable R_{rs} measurements. The sample “station” was defined by the location of a drifter that was deployed to the densest part of the red-tide. The station migrated slightly due to tides. The percentage of dinoflagellates gradually increased for the first two hours from 70% to 75% of the total chlorophyll-*a* pool, decreased at noon to 31%, and then rose again in the early afternoon to 67%. This pattern may represent vertical migration of these motile organisms. Diatoms were predicted to be present in the bay, near the time series and at the mouth of the Salinas River, south of Moss Landing, CA. Cyanophytes were also predicted for the mouth of the Salinas River. Taxon-specific biomass predictions for the other library taxa were negligible.

Table 3.4. MB08. Taxon-specific biomass estimates from PHYDOTax for Rrs collected from the ship in October 2008.

Station	Date	Lat	Lon	Measured [chl-a] (mg m ⁻³)	Predicted Chlorophyll Concentration by Taxonomic Group						
					Dino	Diatom	Hapto	Chloro	Cyano	UPCE	Crypto
C01	10/13/08	36.9000	-121.9600	5.4	1.27	2.64	0.17	0	1.25	0	0.08
C06	10/15/08	36.7416	-121.8200	19.5	4.31	10.26	0.68	0	4.25	0	0
C07	10/17/08	36.8577	-121.8668	13.3	9.31	2.47	0.82	0.06	0	0.64	0
C08	10/17/08	36.8681	-121.8702	5.7	4.28	0.19	0.31	0.35	0	0.57	0
C09	10/17/08	36.6267	-121.8795	8.1	2.51	3.39	0.24	0	1.55	0	0.40
C10	10/17/08	36.8640	-121.8787	6.6	4.45	1.73	0.42	0	0	0	0
C12	10/17/08	36.8717	-121.8849	11.4	5.56	3.49	0.34	0.79	0	1.22	0
C13	10/20/08	36.8793	-121.8745	29.3	17.02	9.40	1.42	0.61	0	0.85	0
C14	10/20/08	36.8826	-121.8827	30.0	13.84	14.85	1.20	0	0.11	0	0
C16	10/23/08	36.9182	-121.8933	18.0	8.11	5.36	0.74	1.76	0	2.03	0
C17	10/23/08	36.8256	-121.8193	7.6	1.85	4.10	0.17	0	1.49	0	0
C18	10/29/08	36.9396	-121.9751	3.8	0.75	1.92	0.09	0	1.04	0	0
C19	10/29/08	36.9349	-121.8821	7.5	2.18	3.50	0.47	0	1.35	0	0

Measured chlorophyll-*a* concentrations were the highest of the four years of the study in 2009 (Table 3.5). Concentrations ranged from 31 to 525 mg m⁻³. One station not reported in the table exceeded 2000 mg m⁻³ chlorophyll-*a*. PHYDOTax predicted that dinoflagellates and diatoms were approximately evenly represented in the bloom, the exception being a station at the Old Salinas River mouth immediately south of Moss Landing. Chlorophyll-*a* concentrations were relatively lower here than at other stations in 2009, but dinoflagellates made up 74% of the assemblage according to PHYDOTax. Unfortunately, radiometric measurements for the northern part of the bay were corrupted and could not be used in the analysis, hence the lack of stations in the red-tide incubator.

Measured chlorophyll-*a* concentrations were much lower in 2010 than in 2009, ranging from 1.2 to 74.2 mg m⁻³ (Table 3.6). Higher concentrations were found in the northern part of the bay, just offshore of Santa Cruz. PHYDOTax predicted that dinoflagellates dominated the assemblage only slightly more than diatoms (~ 40 vs. 30 %) at all but one station in the bay where diatoms were predicted to occupy 45% of the taxon assemblage. This station was located just south of the Santa Cruz Wharf next to the Environmental Sample Processor deployed by researchers from the Monterey Bay Aquarium Research Institute to study the red-tide. Coincidentally, this location was also where a distinctive subsurface diatom bloom was observed just beneath the surface aggregation of dinoflagellates (M. Peacock, pers. comm.).

Table 3.5. MB09. Taxon-specific biomass estimates from PHYDOTax for Rrs collected from the ship in October 2009.

Station	Date	Lat	Lon	Measured [chl-a] (mg m ⁻³)	Predicted Chlorophyll Concentration by Taxonomic Group				
					Dino	Diatom	Hapto	Chloro	Cyano
C06	10/6/09	36.7943	-121.8084	31.0	22.79	3.03	0.94	1.46	0
C08	10/7/09	36.8602	-121.9585	400.0	210.25	129.59	10.88	15.01	0
C09	10/7/09	36.8310	-121.8233	65.0	27.94	25.84	1.33	3.41	0
C11	10/8/09	36.8632	-121.8470	525.0	239.77	202.96	9.22	28.45	0
C12	10/8/09	36.8478	-121.8263	230.0	96.08	89.73	6.84	13.64	0
								23.70	0

Table 3.6. MB10. Taxon-specific biomass estimates from PHYDOTax for Rrs collected from the ship in October 2010.

Station	Date	Lat	Lon	Measured [chl-a] (mg m ⁻³)	Predicted Chlorophyll Concentration by Taxonomic Group				
					Dino	Diatom	Hapto	Chloro	Cyano
E3St1	10/11/10	36.8328	-121.8938	1.2	0.42	0.49	0.04	0	0.14
E12St4	10/12/10	36.9240	-121.9886	74.2	25.67	32.44	1.65	3.66	0
E25St11	10/13/10	36.8661	-121.8518	8.5	5.50	1.24	0.18	0.15	0
E36St16	10/14/10	36.8361	-121.9003	2.1	1.10	0.51	0.07	0.02	0.14
E42St18	10/14/10	36.9322	-121.9693	41.1	20.31	13.11	0.52	1.39	0.00
								2.51	3.25

3.3 Validation

Validation of the model using the synthetic mixtures demonstrated that PHYDOTax accurately predicted taxonomic composition for the mixtures (Table 3.7). The null hypothesis: no difference between predicted and expected proportion, was accepted for all of the taxa ($p > 0.05$).

Table 3.7. Validation of Model - Synthetic Mixtures. Mann-Whitney test results comparing expected phytoplankton proportions to PHYDOTax predictions. A critical p-value of 0.05 was used. > 0.05 indicates PHYDOTax prediction and hypothetical proportion were not statistically different.

Taxon	rank sum	z-value	p-value	H ₀
Dinoflagellate	25187	0.19	0.85	0
Diatom	24682	-0.47	0.64	0
Haptophyte	25188	0.20	0.84	0
Chlorophyte	24774	-0.43	0.67	0
Cyanophyte	25197	0.26	0.80	0
UPCE	24779	-0.42	0.68	0
Cryptophyte	24623	-0.66	0.51	0

In the two-taxon mixtures, PHYDOTax accurately predicted dinoflagellates, diatoms, chlorophytes, cyanophytes, cryptophytes, and UPCE in all instances. When haptophytes were a part of the mixture, PHYDOTax erroneously applied between 1 and 3 % of the mixture to diatoms, applied the remaining 47 - 49% of the mixture to haptophytes, and then 50% to whichever taxon was a part of the mixture. A similar pattern occurred in the three-, five-, and six- taxon mixtures, with negligible mis-apportioning to diatoms when one of the haptophyte taxa was present in the mixture. The predictions for the seven-taxon mixture were an exact match to the expected

proportions. Despite this small failure, the modeled predictions were still statistically the same as the expected proportions. The exception was when the mixture included the spectra for *Emiliana huxleyi*. When *E. huxleyi* was included, PHYDOTax erroneously attributed 50% of the population to diatoms, 30% to cryptophytes, and 15% to haptophytes. This only occurred with *E. huxleyi* in the three-taxon mixtures and not in the two-taxon mixtures and could be due to the unique bio-optics of *E. huxleyi* as a coccolithophorid. Future iterations of PHYDOTax may need to separate *E. huxleyi* from the main haptophyte group in the spectral library.

Field measurements of taxon-specific biomass are reported in Table 3.8 for the cell counts that were measured using the Flow CytoBot in 2006 and by microscope enumeration in 2010. Chlorophyll-*a* concentrations in Table 3.8 match those from Table 3.3 (2006) and Table 3.6 (2010) as both measurements were collected from the same water mass at the same time. Measured dinoflagellate chlorophyll-*a* concentration ranged from 0.32 to 103.4 mg m⁻³. Dinoflagellates represented between 21 and 90% of the taxon assemblage. Diatoms had chlorophyll-*a* concentrations ranging from 1.65 to 160.4 mg m⁻³, with representation between 2 and 75% of the community. Other taxa were present, but generally no greater than 5 to 10% of the total. Curiously, what was considered to be an overwhelmingly massive dinoflagellate-dominated bloom, was actually fairly evenly mixed between dinoflagellates and diatoms at many stations. One exception was the extremely high concentration of dinoflagellates found at a station just south of the Santa Cruz Wharf. This station did not have the highest total chlorophyll-*a* concentration (35 mg m⁻³),

but it did have the highest concentration of dinoflagellates at 90% of the assemblage. The other exception was the intense diatom bloom located near the beach in Aptos, CA. Diatoms were nearly 53% of the assemblage at 160.4 mg m^{-3} chlorophyll-*a*. The patterns of mixed diatom-dinoflagellate assemblages and of the intense diatom bloom at the fringe of the red-tide were found in the PHYDOTax predictions for the R_{rs} measurements from both the ship and imagery.

Table 3.8. Measured taxon-specific chlorophyll concentration. Computed in 2006 using cell counts collected with the FlowCytobot from water collected at each station during the 2006 cruise (Sosik, unpubl. data). Computed in 2010 for diatoms and dinoflagellates from cell counts. Stations and taxa shown include only those that matched PHYDOTax output. (n.d. = no data).

Station	Date	Lat	Lon	Measured Chlorophyll Concentration by Taxonomic Group							
				[chl-a]	(mg m-3)	Dino	Diatom	Hapto	Chlro	Cyano	UPCE
M002	9/5/06	36.8776	-121.8971	7.8	3.39	2.42	0.15	0.30	n.d.	0.67	0.15
M003	9/5/06	36.9385	-121.9543	40.0	24.23	5.12	1.39	1.46	n.d.	5.20	1.39
M006	9/6/06	36.8778	-121.8948	8.0	1.69	3.69	0.39	0.56	n.d.	0.78	0.39
M007	9/7/06	36.8876	-121.8550	300.0	26.58	160.40	16.49	16.49	n.d.	43.80	16.49
M008	9/8/06	36.8341	-121.9009	25.0	18.36	1.65	0.56	0.60	n.d.	1.46	0.58
M009	9/8/06	36.7497	-122.0291	8.0	4.19	2.43	0.14	0.20	n.d.	0.48	0.13
M011	9/11/06	36.8951	-121.9248	50.0	18.49	18.66	1.63	1.89	n.d.	4.44	1.43
M012	9/11/06	36.9087	-121.8582	332.0	103.42	144.13	12.35	12.76	n.d.	31.74	10.50
M013	9/12/06	36.9082	-122.0161	5.7	0.32	4.32	0.20	0.20	n.d.	0.39	0.20
M014	9/12/06	36.8354	-121.9036	39.0	11.71	15.47	1.37	1.66	n.d.	4.12	1.27
M015	9/12/06	36.9154	-121.9770	119.0	40.11	48.85	4.34	5.22	n.d.	10.46	4.34
M016	9/15/06	36.9430	-121.9489	32.0	6.72	17.51	1.97	1.51	n.d.	2.64	1.51
M017	9/15/06	36.9437	-121.9519	35.0	31.59	0.82	0.33	0.39	n.d.	0.91	0.32
E3St1	10/11/10	36.8328	-121.8938	1.2	0.07	1.08	n.d.	n.d.	n.d.	n.d.	n.d.
E12St4	10/12/10	36.9240	-121.9886	74.2	72.70	1.50	n.d.	n.d.	n.d.	n.d.	n.d.
E25St11	10/13/10	36.8661	-121.8518	8.5	7.44	1.06	n.d.	n.d.	n.d.	n.d.	n.d.
E36St16	10/14/10	36.8361	-121.9003	2.1	0.31	1.79	n.d.	n.d.	n.d.	n.d.	n.d.
E42St18	10/14/10	36.9322	-121.9693	41.1	38.20	2.90	n.d.	n.d.	n.d.	n.d.	n.d.

Results of the test of linear regression are plotted in Fig. 3.8 where a trend between measured and modeled taxon-specific biomass is evident for dinoflagellates, diatoms, haptophytes, chlorophytes, and UPCE. The results of the paired t-test indicate that the model successfully predicted dinoflagellates, diatoms, haptophytes, UPCE, and cryptophytes, but not chlorophytes (Table 3.9). The low biomass of chlorophytes and cryptophytes during the period of the cruise may have contributed to the failure to see a trend (cryptophytes) or for the null hypothesis to be rejected (chlorophytes). Cyanophytes could not be validated with field measurements, as there were too few non-zero data-points to make the comparison.

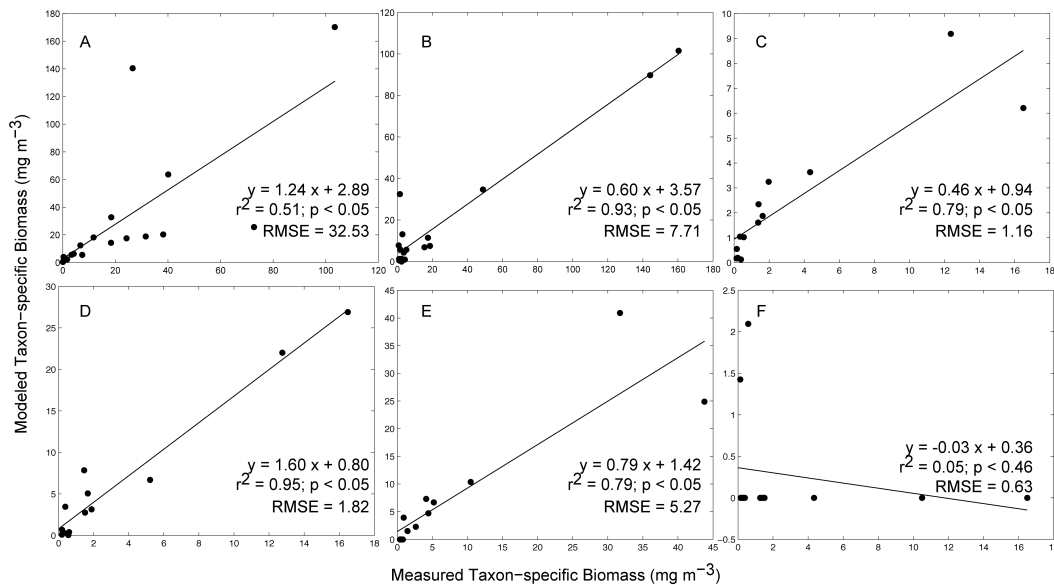


Fig. 3.8. Validation – field samples. Comparison of measured taxon-specific biomass and model estimates from PHYDOTax. Dinoflagellates (2006 and 2010) (A), diatoms (2006 and 2010) (B), haptophytes (C), chlorophytes (D), UPCE (E), and cryptophytes (F) are shown.

Table 3.9. Validation of Model - Field Samples. Regression and paired t-test results comparing taxon-specific chlorophyll biomass from measurements vs. model predictions for COAST 2006 and MB10 (diatoms and dinoflagellates). A critical p-value of 0.05 was used. Paired t-test: > 0.05 indicates measured and modeled values were not statistically different. (n.t. = not testable)

Taxon	Regression					Paired t-test			H ₀
	r ²	slope	intercept	MSE	MSPE	p-value	t-statistic	p-value	
Dinoflagellate	0.51	1.24	2.89	1190.53	1058.25	< 0.05	-1.04	0.31	0
Diatom	0.93	0.60	3.57	66.93	59.50	< 0.05	1.23	0.23	0
Haptophyte	0.79	0.46	0.94	1.60	1.36	< 0.05	0.92	0.38	0
Chlorophyte	0.95	1.60	0.80	3.92	3.32	< 0.05	-2.74	0.02	1
Cyanophyte	n.t.	n.t.	n.t.	n.t.	n.t.	n.t.	n.t.	n.t.	n.t.
UPCE	0.79	0.79	1.42	32.78	27.73	< 0.05	0.20	0.84	0
Cryptophyte	0.05	-0.03	0.36	0.47	0.40	0.46	1.90	0.08	0

3.4 Imagery

Chlorophyll-*a* biomass was estimated to be very high in the red-tide incubator of the northern Monterey Bay in the 2006 imagery (Fig. 3.9). The bloom was concentrated in two patches, one close to shore near Aptos, CA and another just offshore, parallel to the shore and the prevailing internal wave fronts that are commonly present at that location [J. P. Ryan *et al.*, 2009]. Surface concentrations of chlorophyll-*a* ranged from near zero offshore to more than 400 mg m⁻³ in the densest part of the bloom, as confirmed by water samples collected during the research cruise.

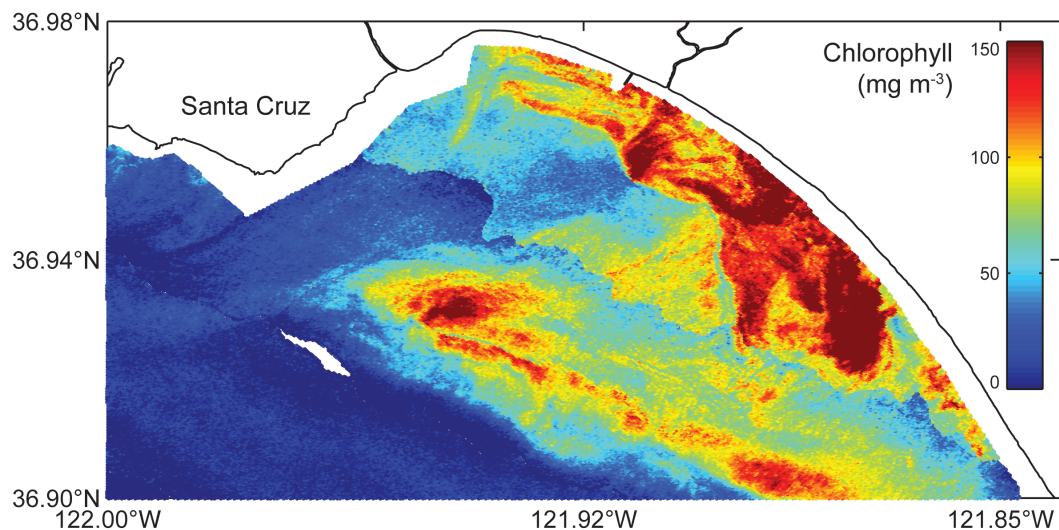


Fig. 3.9. Derived Chlorophyll-*a* Biomass – imagery. Chlorophyll-*a* was derived from fluorescence line height (FLH) using the relationship between *in situ* chorophyll-*a* measurements and FLH computed from *in situ* Rrs measurements. Relationship was applied to imagery FLH to derive chorophyll-*a* biomass. Image collected September 12, 2006 using SAMSOM Hyper-spectral airborne sensor.

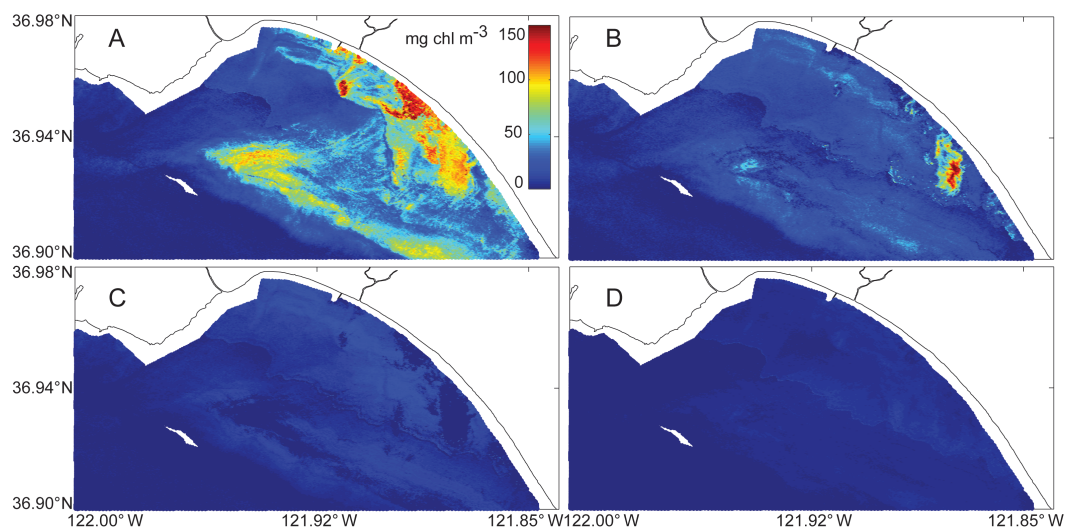


Fig. 3.10. Predicted taxon-specific biomass – 2006 Imagery. Estimates of the chlorophyll-*a* concentration represented by phytoplankton taxon; (A) dinoflagellates, (B) diatoms, (C) cyanobacteria, (D) haptophytes. Image collected September 12, 2006 using SAMSOM Hyper-spectral airborne sensor.

Water measurements indicate that the bloom was dominated by the dinoflagellate *Akashiwo sanguinea*. PHYDOTax predicted that dinoflagellates were the primary taxon present in the bloom region with 40 to 90% of the taxon-assemblage composed of this group (Fig. 3.10A). Dinoflagellate-specific chlorophyll-*a* biomass reached 182 mg m⁻³ in some regions and ranged between 15 and 117 mg m⁻³ in most parts of the bloom. PHYDOTax predicted the presence of diatoms within the dinoflagellate bloom (~20%), but at lower concentrations (3.9 to 61 mg m⁻³), and at the periphery of the bloom at concentrations as high as 179 mg m⁻³ (Fig. 3.10B). This pattern is borne out in the water measurements collected at stations within the bloom during the research cruise, though only two stations coincided with the time of image capture and at locations outside of the image boundary. The presence of all other taxa in the library was negligible (Fig. 3.10C & 3.15D). Haptophytes, chlorophytes, UPCE, and cryptophytes were predicted to have median chlorophyll-*a* concentrations of 6.6, 0, 0, and 8.3 mg m⁻³ respectively. Cyanophytes were predicted to have a median chlorophyll-*a* concentration of 9.7 mg m⁻³, mostly co-located with the intense dinoflagellate bloom.

4.0 Discussion

In this paper we have presented a bio-optical model to simultaneously discriminate multiple phytoplankton taxa from hyperspectral remote sensing reflectance spectra. This phytoplankton discriminator algorithm is a robust tool for quantifying taxon-specific biomass in optically complex, case 2 waters. Validation confirms that

PHYDOTax can distinguish among diatoms, dinoflagellates, haptophytes, cryptophytes, chlorophytes, cyanophytes, and UPCE. PHYDOTax is the first ocean color algorithm to discriminate between diatoms and dinoflagellates. The generally accepted paradigm has been that these two taxa cannot be differentiated from each other because of the overlap in pigment composition or similarities in light absorption spectra [Dierssen *et al.*, 2006]. This novel algorithm is a promising tool to partition the phytoplankton biomass in the coastal environment where diatoms and dinoflagellates occur together and may support different ecosystems or occupy different niches within a harmful algal bloom.

In addition to developing a new algorithm to distinguish algae from ocean color data, this is the first published study demonstrating the feasibility of measuring backscattering directly from large-volume phytoplankton cultures. Backscattering measurements were collected to more accurately model R_{rs} of the pure cultures. These measurements are important for the ocean color community to better characterize IOPs of taxonomically pure end-members [Nair *et al.*, 2008].

4.1 Comparison with existing algorithms

When compared to existing algorithms, PHYDOTax has several advantages over its predecessors. PHYDOTax's conceptual ancestor, CHEMTAX, is limited in spatial resolution as it is implemented on pigment data collected *in situ*. CHEMTAX credibly estimates taxon-assemblage. However, its input requirements are onerous: water must first be collected *in situ*; the pigments extracted and measured using high-

performance liquid chromatography by a trained technician; then the expected library taxa and pigment ratios tuned to a particular habitat or region; followed by execution of the algorithm [Mackey *et al.*, 1996]. Assignment to an incorrect algal taxon is possible simply by choosing pigment ratios tuned to a different geographic region or the wrong suite of expected algal taxa [Lewitus *et al.*, 2005; Mackey *et al.*, 1996]. Compared to PHYDOTax, application of this model is limited in spatial and temporal scale as it was designed to validate taxon-composition from whole water samples, and not from remote observations from moorings or satellites.

An active and successful research campaign has been the detection of the toxic dinoflagellate *Karenia brevis* on the west Florida shelf using remote ocean color observations from moorings [Stumpf *et al.*, 2003], autonomous underwater vehicles [Robbins *et al.*, 2006], airborne sensors [Cannizzaro *et al.*, 2008], and satellites [Hu *et al.*, 2005; Shanmugam, 2011; Stumpf *et al.*, 2003; Tomlinson *et al.*, 2009]. Bio-optical algorithm development has been prolific. An early model was a two-dimensional spectral analysis technique to determine similarity [Millie *et al.*, 1997]. *Karenia brevis* contains the pigment bio-marker gyroxanthin-diester, which has distinctive absorption properties. At only 5% of the magnitude of the spectrum [Millie *et al.*, 1995], it is a relatively weak signal and is overwhelmed by chlorophyll-*c* and fucoxanthin. Historically, this algorithm has been used with *in situ* water samples, but with recent advances in decomposing IOPs from hyperspectral ocean color imagery [Lee and Carder, 2004] these comparisons can be made over much larger spatial scales. Another algorithm that exploits the contrast of the unique properties of *K.*

brevis against an optically different background is that developed by Cannizzaro and collaborators [Cannizzaro *et al.*, 2008; Cannizzaro *et al.*, 2009]. This model distinguishes *K. brevis* by its distinctively low chlorophyll-specific particulate backscattering coefficient at 550 nm ($\leq 0.0045 \text{ m}^2 \text{ mg}^{-1}$) [Cannizzaro *et al.*, 2009]. This differs dramatically from the type of phytoplankton that may be present in the case 1 waters where *K. brevis* is typically found. Using a large hyperspectral dataset for the WFS as a test, this model accurately discriminated *K. brevis* blooms from non-blooms 99% of the time [Cannizzaro *et al.*, 2009]. Both of these *K. brevis*-specific algorithms were developed with hyperspectral data to discriminate just one phytoplankton species, albeit a noxious one, from a background of non-bloom waters. These, and other remote sensing algorithms for the WFS, have been successful and a necessary “proof-of-concept” that ocean color can be used to identify harmful algae in case 1 waters. A logical next step addressed in the present is to detect algae in more optically complex, case 2 waters, or in waters with a plurality of algal taxa influencing the ecosystem and bio-optics.

Two bio-optical algorithms that distinguish red-tides in optically complex waters have been applied to northeast-Asia coastal waters [Ahn and Shanmugam, 2006], the Arabian Sea and Gulf of Oman, and the West Florida Shelf as a test of case 1 waters [Shanmugam, 2011]. These two algorithms, the red-tide index (RI) and the algal bloom index (ABI) use an empirical relationship between chlorophyll-*a* concentration and band-ratios of ocean color to detect red-tides. They were developed to differentiate dinoflagellate blooms upon a background of turbid water and other

phytoplankton species using existing multispectral satellite imagery from SeaWiFS or MODIS [*Ahn and Shanmugam*, 2006; *Shanmugam*, 2011]. These algorithms successfully identify the presence of a red-tide in both the case 1 and case 2 water types. Both band-ratio methods fail with incorrect chlorophyll-*a* estimates. So, the choice of chlorophyll-*a* algorithm or the atmospheric correction parameters used in processing the imagery can affect algorithm performance [*Shanmugam*, 2011]. This is particularly a concern in near-shore environments where the atmospheric composition can differ greatly from near-shore to offshore. Despite these caveats, the algorithms are effective at distinguishing red-tides in optically complex waters and can do so with existing satellites. However, they are limited to a bulk estimate of the red-tide and do not distinguish among other coincident phytoplankton taxa that may contribute to the deleterious effects of a bloom.

The phytoplankton classification algorithm PHYSAT does simultaneously solve for multiple phytoplankton taxa using multispectral ocean color imagery [*Alvain et al.*, 2005]. It is effective at characterizing the taxonomic composition in case 1 waters of the global ocean [*Alvain et al.*, 2008; *d'Ovidio et al.*, 2010] and could be a valuable algorithm for describing the partitioning of carbon flow [*Masotti et al.*, 2011] in several biogeochemical provinces including the north Atlantic and the Southern Ocean [*Alvain et al.*, 2008]. PHYSAT and PHYDOTax are similar in that they solve for multiple taxa in one iteration of the algorithm. They differ in the taxonomic composition of the signature library; the approach to development – PHYSAT is empirical and PHYDOTax is semi-analytical; and the water types where

they can be applied. PHYSAT will be technically challenged to distinguish among some taxa traditionally grouped in the brown color group [Beutler *et al.*, 2002] which includes diatoms and dinoflagellates. PHYSAT uses the relationship between diagnostic pigment bio-markers and water-leaving radiance to classify groups: Pigment overlap in dinoflagellates and diatoms discourages delimiting the two groups [Dierssen *et al.*, 2006]. Because PHYDOTax uses R_{rs} , which incorporates backscattering, it does not suffer from the pigment overlap problem. Pigment composition must be unequivocal among the phytoplankton taxa in order to clearly characterize the different groups using PHYSAT. Further increases in algal groups may be limited by vague pigment distinctions in the remaining taxa not yet characterized. Another limitation is extending PHYSAT to optically complex waters where higher turbidity, CDOM, and phytoplankton are conflated in one water-leaving radiance spectrum. A semi-analytical approach that includes a range of concentrations of non-algal particles or CDOM in the library building spectra may more closely approximate the bio-optics of a phytoplankton bloom in case 2 waters. In its current state, PHYDOTax has non-varying a_{NAP} and a_{CDOM} in its signature library; however, it has the potential to include such variability because of its semi-analytical approach to modeling library spectra. Even without including variability in non-algal particles and CDOM, PHYDOTax can predict the composition of phytoplankton taxa in the optically complex waters of Monterey Bay, CA.

4.2 Implications for PFT Modeling and HAB Monitoring

PHYDOTax successfully discriminates phytoplankton taxa in coastal waters. It may be possible to apply the algorithm to case 1 waters with future enhancements to the signature library to include *Prochlorococcus*, *Trichodesmium*, and other phytoplankton more typical of the open ocean. Plankton functional type models vary in complexity from relatively simple NPZD models with one to three phytoplankton size-classes to a more complex 78 phytoplankton-type model (i.e. DARWIN) [Follows *et al.*, 2007]. High-complexity models are alluring as they promise to explain the ecosystem more thoroughly. Validating these models is problematic without an equal number of independent validation observations as there are input variables [T R Anderson, 2005]. Satellite observations have historically provided relatively few of the independent observations needed to validate models. Recent work by Alvain *et al.* [Alvain *et al.*, 2005; Alvain *et al.*, 2008; Alvain *et al.*, 2006] has made it possible to observe some plankton functional types in the open ocean. PHYDOTax may do the same for the coastal ocean. While PHYDOTax will never meet the 78 input parameter threshold for independent validation, it does predict more phytoplankton groups than existing algorithms, and more signature library taxa could be added to the model in the future. For implementations of DARWIN, or simplifications of DARWIN, in the CCS [Goebel *et al.*, 2010], PHYDOTax could be a viable tool to produce validation observations. Ultimately, one goal of PFTs is to constrain estimates of carbon flow. It may soon be possible to validate those predictions in the CCS with increased availability of hyperspectral imagery along the

CA coast using the Hyperspectral Imager for the Coastal Ocean (HICO™) imaging spectrometer on the International Space Station.

Taxonomically, PHYDOTax discriminates to the family level or higher. Because of shared pigments, morphology, and cell wall material within taxa, it is unlikely that the algorithm will ever differentiate within the existing taxa-- the exception being haptophytes and dinoflagellates. These two phylogenetically and bio-optically diverse groups [Falkowski *et al.*, 2004; Keeling, 2004; Lewitus *et al.*, 2005] may be separated to improve performance of the algorithm. PHYDOTax does not resolve to the species level, so it cannot be used to directly detect and monitor a HAB. However, it can be used to identify the dominant taxon within a bloom. As evidenced in this study (Fig. 3.10), PHYDOTax described a mixed dinoflagellate-diatom bloom in 2006. The ability of the model to simultaneously resolve dinoflagellates and diatoms could aid in describing taxon patchiness within a larger bloom. *In situ* measurements confirmed the small diatom bloom found at the periphery of the larger red-tide (Fig. 3.10B). Prior to PHYDOTax; chlorophyll-*a*, light absorption, and particulate backscattering could be discerned from the hyperspectral R_{rs} imagery [Lee and Carder, 2004]. Conclusions could be drawn as to the likelihood of taxa within the bloom, but no further predictions could be made. Using PHYDOTax, knowledge of the taxonomic composition of the HAB could improve decision making and adaptive sampling of the bloom.

4.3 Limitations and Future Work

PHYDOTax has its limitations, and like its conceptual predecessor, CHEMTAX, should not be treated like a “black box.” Like CHEMTAX, PHYDOTax is an over determined solution and therefore the number of independent variables retrieved (i.e. expected library taxa) cannot exceed the number of wavelengths used in the algorithm (twenty-three wavebands). In addition, some *a priori* knowledge of the expected taxonomic composition is needed to select the signature library taxa to use in the model-runs. In the future, the hope is to add more library taxa to the signature library to extend the utility of PHYDOTax beyond the seven taxa currently in it. The existing library is composed of taxa found mostly in the coastal ocean of Monterey Bay. A next step is to include *Prochlorococcus* and *Trichodesmium*, and a wider diversity of eukaryotes including chrysophytes and silicoflagellates. Additionally, to include more species within the haptophyte and dinoflagellate groups (beyond the three in each) to more adequately represent the wide range of bio-optical subtypes in those two groups [Falkowski *et al.*, 2004; Keeling, 2004; Lewitus *et al.*, 2005]. A third limitation is that the algorithm uses hyperspectral data. One sensor, the Hyperion Imager aboard NASA’s EO-1 satellite, has the spectral and spatial resolution needed to accommodate PHYDOTax. Imagery from this sensor is captured by on-demand requests from approved research projects for both terrestrial and aquatic systems. Demand by the many stakeholders limits the availability of imagery from the coastal ocean. Until recently, Hyperion images were very costly. With the launch of HICO™, repeated satellite retrievals over the coastal ocean are now available to ask relevant

scientific questions using PHYDOTax. The limited availability of hyperspectral imagery does not preclude the implementation of PHYDOTax on data-sets from mooring arrays that measure surface remote sensing reflectance. So, while HICO data may be limited in its coverage or temporal resolution, taxon-specific discrimination is currently possible with existing instrumented moorings.

The future of ocean color remote sensing is gradually moving towards hyperspectral imagers with the temporal and spatial resolution found on MODIS. Hyperspectral sensors are expensive to develop and the anticipated computing and data-storage needs are very costly. Not surprisingly, government entities equivocate in embracing missions to launch hyperspectral imagers into space. With little commitment to launch hyperspectral imagers, the research community is reluctant to develop and test hyperspectrally-based algorithms. However, within the last five years the impasse has broken; the number of algorithms has increased [*Cannizzaro et al.*, 2008; *Craig et al.*, 2006; *Torrecilla et al.*, 2011]. PHYDOTax is an example of one, and also provides a valuable lesson: The need for “hyperspectral” may not require 1 nm resolution with sub-nanometer bandwidth. PHYDOTax operates at 10 nm resolution with a ~2 nm bandwidth and can discriminate among taxa previously thought indivisible. If other bio-optical algorithms can perform at similar spectral resolution, then it may be possible to launch a lower resolution sensor that still affords the computational skill needed for spectral analysis, but at a resolution that is affordable to develop and maintain.

5.0 Acknowledgements

This work was funded by the NOAA GOES-R COAST project, NESDIS-NASA UARC Award (TO.030.6.MD.D-Kudela), UC-Santa Cruz Chancellor's Dissertation Year Fellowship (SP), Dr. Earl H. Myers and Ethel M. Myers Oceanographic and Marine Biology Trust (SP). We thank the captain and crew of the *R/V John H. Martin* for services rendered throughout the four years of field-work. SP wishes to especially thank Clarissa Anderson, Misty Blakely, Taylor Crockford, Meredith Howard, Maria Kavanaugh, Rick Pasetto, G. Jason Smith, and Rick Stumpf for assistance. We thank Christopher Edwards and the anonymous reviewers for their time and attention given to this manuscript.

Literature Cited

- Abbott, M. R., and R. M. Letelier (2006), Algorithm theoretical basis document: Chlorophyll fluorescence (MODIS product number 20)*Rep.*
- Ahn, Y. H., and P. Shanmugam (2006), Detecting the red tide algal blooms from satellite ocean color observations in optically complex Northeast-Asia Coastal waters, *Remote Sensing of Environment*, 103(4), 419-437.
- Alvain, S., C. Moulin, Y. Dandonneau, and F. M. Breon (2005), Remote sensing of phytoplankton groups in case 1 waters from global SeaWiFS imagery, *Deep-Sea Research Part I-Oceanographic Research Papers*, 52(11), 1989-2004.
- Alvain, S., C. Moulin, Y. Dandonneau, and H. Loisel (2008), Seasonal distribution and succession of dominant phytoplankton groups in the global ocean: A satellite view, *Global Biogeochemical Cycles*, 22(3).
- Alvain, S., C. Moulin, Y. Dandonneau, H. Loisel, and F. M. Breon (2006), A species-dependent bio-optical model of case I waters for global ocean color processing, *Deep-Sea Research Part I-Oceanographic Research Papers*, 53(5), 917-925.
- Anderson, D. M., P. Hoagland, Y. Kaoru, and A. W. White (2000), Economic impacts from harmful algal blooms (HABs) in the United States*Rep.*, Woods Hole Oceanographic Institution, Woods Hole, MA.
- Anderson, T. R. (2005), Plankton functional type modelling: running before we can walk?, *Journal of Plankton Research*, 27(11), 1073-1081.
- Arar, E. J., and G. B. Collins (1997), Method 445.0: In vitro determination of chlorophyll a and pheophytin a in marine and freshwater algae by fluorescence, edited by U. S. E. P. Agency, Cincinnati, Ohio.
- Behrenfeld, M. J., and P. G. Falkowski (1997), Photosynthetic rates derived from satellite-based chlorophyll concentration, *Limnology and Oceanography*, 42(1), 1-20.
- Beutler, M., K. H. Wiltshire, B. Meyer, C. Moldaenke, C. Luring, M. Meyerhofer, U. P. Hansen, and H. Dau (2002), A fluorometric method for the differentiation of algal populations in vivo and in situ, *Photosynthesis Research*, 72(1), 39-53.
- Breaker, L. C., and W. W. Broenkow (1994), The circulation of Monterey Bay and related processes, *Oceanography and Marine Biology*, 32, 1 - 64.
- Cannizzaro, J. P., K. L. Carder, F. R. Chen, C. A. Heil, and G. A. Vargo (2008), A novel technique for detection of the toxic dinoflagellate, Karenia brevis, in the Gulf

of Mexico from remotely sensed ocean color data, *Continental Shelf Research*, 28(1), 137-158.

Cannizzaro, J. P., C. M. Hu, D. C. English, K. L. Carder, C. A. Heil, and F. E. Muller-Karger (2009), Detection of Karenia brevis blooms on the west Florida shelf using in situ backscattering and fluorescence data, *Harmful Algae*, 8(6), 898-909.

Carder, K. L., R. G. Steward, G. R. Harvey, and P. B. Ortner (1989), Marine Humic and Fulvic-Acids - Their Effects on Remote-Sensing of Ocean Chlorophyll, *Limnology and Oceanography*, 34(1), 68-81.

Ciotti, A. M., J. J. Cullen, and M. R. Lewis (1999), A semi-analytical model of the influence of phytoplankton community structure on the relationship between light attenuation and ocean color, *Journal of Geophysical Research-Oceans*, 104(C1), 1559-1578.

Ciotti, A. M., M. R. Lewis, and J. J. Cullen (2002), Assessment of the relationships between dominant cell size in natural phytoplankton communities and the spectral shape of the absorption coefficient, *Limnology and Oceanography*, 47(2), 404-417.

Claustre, H. (1994), THE TROPHIC STATUS OF VARIOUS OCEANIC PROVINCES AS REVEALED BY PHYTOPLANKTON PIGMENT SIGNATURES, *Limnology and Oceanography*, 39(5), 1206-1210.

Cleveland, J. S., and A. D. Weidemann (1993), QUANTIFYING ABSORPTION BY AQUATIC PARTICLES - A MULTIPLE-SCATTERING CORRECTION FOR GLASS-FIBER FILTERS, *Limnology and Oceanography*, 38(6), 1321-1327.

Craig, S. E., S. E. Lohrenz, Z. P. Lee, K. L. Mahoney, G. J. Kirkpatrick, O. M. Schofield, and R. G. Steward (2006), Use of hyperspectral remote sensing reflectance for detection and assessment of the harmful alga, Karenia brevis, *Applied Optics*, 45(21), 5414-5425.

d'Ovidio, F., S. De Montec, S. Alvain, Y. Dandonneau, and M. Levy (2010), Fluid dynamical niches of phytoplankton types, *Proceedings of the National Academy of Sciences of the United States of America*, 107(43), 18366-18370.

Davis, C., and W. P. Bissett (2007), Characterization of a harmful algal bloom in Monterey Bay, CA using airborne hyperspectral imagery, in *Hyperspectral Imaging and Sounding of the Environment (HISE)*, edited, Optical Society of America (OSA), Santa Fe, NM.

Devred, E., S. Sathyendranath, V. Stuart, and T. Platt (2011), A three component classification of phytoplankton absorption spectra: Application to ocean-color data, *Remote Sensing of Environment*, 115(9), 2255-2266.

Dierssen, H. M., R. M. Kudela, J. P. Ryan, and R. C. Zimmerman (2006), Red and black tides: Quantitative analysis of water-leaving radiance and perceived color for phytoplankton, colored dissolved organic matter, and suspended sediments, *Limnology and Oceanography*, 51(6), 2646 - 2659.

Falkowski, P. G., M. E. Katz, A. H. Knoll, A. Quigg, J. A. Raven, O. Schofield, and F. J. R. Taylor (2004), The evolution of modern eukaryotic phytoplankton, *Science*, 305(5682), 354-360.

Fawcett, A., G. C. Pitcher, S. Bernard, A. D. Cembella, and R. M. Kudela (2007), Contrasting wind patterns and toxicogenic phytoplankton in the southern Benguela upwelling system, *Marine Ecology-Progress Series*, 348, 19-31.

Follows, M. J., S. Dutkiewicz, S. Grant, and S. W. Chisholm (2007), Emergent biogeography of microbial communities in a model ocean, *Science*, 315(5820), 1843-1846.

Goebel, N. L., C. A. Edwards, J. P. Zehr, and M. J. Follows (2010), An emergent community ecosystem model applied to the California Current System, *Journal of Marine Systems*, 83(3-4), 221-241.

Gordon, H. R., J. W. Brown, O. B. Brown, R. H. Evans, and D. K. Clark (1983), Nimbus-7 Czcs - Reduction of Its Radiometric Sensitivity with Time, *Applied Optics*, 22(24), 3929-3931.

Hommersom, A., M. R. Wernand, S. Peters, M. A. Eleveld, H. J. van der Woerd, and J. de Boer (2011), Spectra of a shallow sea-unmixing for class identification and monitoring of coastal waters, *Ocean Dynamics*, 61(4), 463-480.

Honner, S., R. M. Kudela, and E. Handler (2010), Bilateral mastoiditis from red tide exposure, *Journal of Emergency Medicine*.

Hu, C. M., F. E. Muller-Karger, C. Taylor, K. L. Carder, C. Kelble, E. Johns, and C. A. Heil (2005), Red tide detection and tracing using MODIS fluorescence data: A regional example in SW Florida coastal waters, *Remote Sensing of Environment*, 97(3), 311-321.

Jessup, D. A., M. A. Miller, J. P. Ryan, H. M. Nevins, H. A. Kerkering, A. Mekebri, D. B. Crane, T. A. Johnson, and R. M. Kudela (2009), Mass Stranding of Marine Birds Caused by a Surfactant-Producing Red Tide, *Plos One*, 4(2).

Jester, R., K. Lefebvre, G. Langlois, V. Vigilant, K. Baugh, and M. W. Silver (2009), A shift in the dominant toxin-producing algal species in central California alters phycotoxins in food webs, *Harmful Algae*, 8(2), 291-298.

Kana, T. M., P. M. Glibert, R. Goericke, and N. A. Welschmeyer (1988), ZEAXANTHIN AND BETA-CAROTENE IN SYNECHOCOCCUS WH7803 RESPOND DIFFERENTLY TO IRRADIANCE, *Limnology and Oceanography*, 33(6), 1623-1627.

Keeling, P. J. (2004), Diversity and evolutionary history of plastids and their hosts, *American Journal of Botany*, 91(10), 1481-1493.

Kirk, J. T. O. (1994), *Light and photosynthesis in aquatic ecosystems*, 509 pp., Cambridge University Press, New York.

Kostadinov, T. S., D. A. Siegel, and S. Maritorena (2009), Retrieval of the particle size distribution from satellite ocean color observations, *Journal of Geophysical Research-Oceans*, 114.

Kudela, R. M., J. P. Ryan, M. D. Blakely, J. Q. Lane, and T. D. Peterson (2008), Linking the physiology and ecology of *Cochlodinium* to better understand harmful algal bloom events: A comparative approach, *Harmful Algae*, 7(3), 278-292.

Lee, Z. P., and K. L. Carder (2004), Absorption spectrum of phytoplankton pigments derived from hyperspectral remote-sensing reflectance, *Remote Sensing of Environment*, 89(3), 361-368.

Lee, Z. P., K. L. Carder, and R. A. Arnone (2002), Deriving inherent optical properties from water color: a multiband quasi-analytical algorithm for optically deep waters, *Applied Optics*, 41(27), 5755-5772.

Lewitus, A. J., D. L. White, R. G. Tymowski, M. E. Geesey, S. N. Hymel, and P. A. Noble (2005), Adapting the CHEMTAX method for assessing phytoplankton taxonomic composition in southeastern US estuaries, *Estuaries*, 28(1), 160-172.

Mackey, M. D., D. J. Mackey, H. W. Higgins, and S. W. Wright (1996), CHEMTAX - A program for estimating class abundances from chemical markers: Application to HPLC measurements of phytoplankton, *Marine Ecology-Progress Series*, 144(1-3), 265-283.

Martin Traykovski, L. V., and H. M. Sosik (2003), Feature-based classification of optical water types in the Northwest Atlantic based on satellite ocean color data, *J. Geophys. Res.*, 108(C5), -.

- Masotti, I., C. Moulin, S. Alvain, L. Bopp, A. Tagliabue, and D. Antoine (2011), Large-scale shifts in phytoplankton groups in the Equatorial Pacific during ENSO cycles, *Biogeosciences*, 8(3), 539-550.
- Mazzillo, F., J. Ryan, and M. Silver (2011), Parasitism as a biological control agent of dinoflagellate blooms in the California Current System, *Harmful Algae*, 10, 763 - 773.
- Millie, D. F., G. J. Kirkpatrick, and B. T. Vinyard (1995), RELATING PHOTOSYNTHETIC PIGMENTS AND IN-VIVO OPTICAL-DENSITY SPECTRA TO IRRADIANCE FOR THE FLORIDA RED-TIDE DINOFLAGELLATE GYMNOODINIUM BREVE, *Marine Ecology-Progress Series*, 120(1-3), 65-75.
- Millie, D. F., O. M. Schofield, G. J. Kirkpatrick, G. Johnsen, P. A. Tester, and B. T. Vinyard (1997), Detection of harmful algal blooms using photopigments and absorption signatures: A case study of the Florida red tide dinoflagellate, *Gymnodinium breve*, *Limnology and Oceanography*, 42(5), 1240-1251.
- Mobley, C. D. (1994), *Light and Water. Radiative Transfer in Natural Waters*, Academic, New York.
- Mobley, C. D., and L. K. Sundman (2008), Hydrolight 5 Ecolight 5 Users' GuideRep., Sequoia Scientific, Inc., Bellevue, WA.
- Moore, T. S., J. W. Campbell, and H. Feng (2001), A fuzzy logic classification scheme for selecting and blending satellite ocean color algorithms, *Ieee Transactions on Geoscience and Remote Sensing*, 39(8), 1764-1776.
- Morel, A., and L. Prieur (1977), Analysis of Variations in Ocean Color, *Limnology and Oceanography*, 22(4), 709-722.
- Nair, A., S. Sathyendranath, T. Platt, J. Morales, V. Stuart, M. H. Forget, E. Devred, and H. Bouman (2008), Remote sensing of phytoplankton functional types, *Remote Sensing of Environment*, 112(8), 3366-3375.
- O'Reilly, J. E., S. Maritorena, B. G. Mitchell, D. A. Siegel, K. L. Carder, S. A. Garver, M. Kahru, and C. McClain (1998), Ocean color chlorophyll algorithms for SeaWiFS, *Journal of Geophysical Research-Oceans*, 103(C11), 24937-24953.
- Olson, R. J., and H. M. Sosik (2007), A submersible imaging-in-flow instrument to analyze nano-and microplankton: Imaging FlowCytobot, *Limnology and Oceanography-Methods*, 5, 195-203.

- Pennington, J. T., and F. P. Chavez (2000), Seasonal fluctuations of temperature, salinity, nitrate, chlorophyll and primary production at station H3/M1 over 1989 - 1996 in Monterey Bay, California, *Deep-Sea Research II*, 47, 947 - 973.
- Pope, R. M., and E. S. Fry (1997), Absorption spectrum (380-700 nm) of pure water .2. Integrating cavity measurements, *Applied Optics*, 36(33), 8710-8723.
- Robbins, I. C., G. J. Kirkpatrick, S. M. Blackwell, J. Hillier, C. A. Knight, and M. A. Moline (2006), Improved monitoring of HABs using autonomous underwater vehicles (AUV), *Harmful Algae*, 5(6), 749-761.
- Ryan, J. P., A. M. Fischer, R. M. Kudela, J. F. R. Gower, S. A. King, R. Marin, and F. P. Chavez (2009), Influences of upwelling and downwelling winds on red tide bloom dynamics in Monterey Bay, California, *Continental Shelf Research*, 29(5-6), 785-795.
- Ryan, J. P., H. M. Dierssen, R. M. Kudela, C. A. Scholin, K. S. Johnson, J. M. Sullivan, A. M. Fischer, E. V. Rienecker, P. R. McEnaney, and F. P. Chavez (2005), Coastal ocean physics and red tides: an example from Monterey Bay, California, *Oceanography*, 18(2), 246 - 255.
- Ryan, J. P., J. F. R. Gower, S. A. King, W. P. Bissett, A. M. Fischer, R. M. Kudela, Z. Kolber, F. Mazzillo, E. V. Rienecker, and F. P. Chavez (2008), A coastal ocean extreme bloom incubator, *Geophysical Research Letters*, 35(12).
- Sathyendranath, S., G. Cota, V. Stuart, H. Maass, and T. Platt (2001), Remote sensing of phytoplankton pigments: a comparison of empirical and theoretical approaches, *International Journal of Remote Sensing*, 22(2-3), 249-273.
- Sathyendranath, S., L. Watts, E. Devred, T. Platt, C. Caverhill, and H. Maass (2004a), Discrimination of diatoms from other phytoplankton using ocean-colour data, *Marine Ecology-Progress Series*, 272, 59-68.
- Sathyendranath, S., et al. (2004b), A multispectral remote sensing study of coastal waters off Vancouver Island, *International Journal of Remote Sensing*, 25(5), 893-919.
- Scholin, C., et al. (2009), Remote Detection of Marine Microbes, Small Invertebrates, Harmful Algae, and Biotoxins Using the Environmental Sample Processor (Esp), *Oceanography*, 22(2), 158-167.
- Scholin, C. A., et al. (2000), Mortality of sea lions along the central California coast linked to a toxic diatom bloom, *Nature*, 403(6765), 80-84.

Shanmugam, P. (2011), A new bio-optical algorithm for the remote sensing of algal blooms in complex ocean waters, *Journal of Geophysical Research-Oceans*, 116.

Smayda, T. J. (1997), Harmful algal blooms: Their ecophysiology and general relevance to phytoplankton blooms in the sea, *Limnology and Oceanography*, 42(5), 1137-1153.

Smayda, T. J., and C. S. Reynolds (2001), Community assembly in marine phytoplankton: application of recent models to harmful dinoflagellate blooms, *Journal of Plankton Research*, 23(5), 447-461.

Sosik, H. M., and R. J. Olson (2007), Automated taxonomic classification of phytoplankton sampled with imaging-in-flow cytometry, *Limnology and Oceanography-Methods*, 5, 204-216.

Stramski, D., and D. A. Kiefer (1991), LIGHT-SCATTERING BY MICROORGANISMS IN THE OPEN OCEAN, *Progress in Oceanography*, 28(4), 343-383.

Stumpf, R. P. (2001), Applications of satellite ocean color sensors for monitoring and predicting harmful algal blooms, *Human and Ecological Risk Assessment*, 7(5), 1363-U1315.

Stumpf, R. P., M. E. Culver, P. A. Tester, M. Tomlinson, G. J. Kirkpatrick, B. A. Pederson, E. Truby, V. Ransibrahmanakul, and M. Soracco (2003), Monitoring *Karenia brevis* blooms in the Gulf of Mexico using satellite ocean color imagery and other data, *Harmful Algae*, 2(2), 147-160.

Subramaniam, A., C. W. Brown, R. R. Hood, E. J. Carpenter, and D. G. Capone (2002), Detecting *Trichodesmium* blooms in SeaWiFS imagery, *Deep-Sea Research Part II-Topical Studies in Oceanography*, 49(1-3), 107-121.

Tomlinson, M. C., T. T. Wynne, and R. P. Stumpf (2009), An evaluation of remote sensing techniques for enhanced detection of the toxic dinoflagellate, *Karenia brevis*, *Remote Sensing of Environment*, 113(3), 598-609.

Torrecilla, E., D. Stramski, R. A. Reynolds, E. Millan-Nunez, and J. Piera (2011), Cluster analysis of hyperspectral optical data for discriminating phytoplankton pigment assemblages in the open ocean, *Remote Sensing of Environment*, 115(10), 2578-2593.

Uitz, J., H. Claustre, A. Morel, and S. B. Hooker (2006), Vertical distribution of phytoplankton communities in open ocean: An assessment based on surface chlorophyll, *Journal of Geophysical Research-Oceans*, 111(C8).

Zar, J. H. (1996), *Biostatistical Analysis*, 3rd ed., Prentice Hall College Div, Upper Saddle River, NJ.